Cellular convection with finite amplitude in a rotating fluid

By G. VERONIS
Woods Hole Oceanographic Institution, Woods Hole, Massachusetts

(Received 3 July 1958)

When a rotating layer of fluid is heated uniformly from below and cooled from above, the onset of instability is inhibited by the rotation. The first part of this paper treats the stability problem as it was considered by Chandrasekhar (1953), but with particular emphasis on the physical interpretation of the results. It is shown that the time-dependent (overstable) motions occur because they can reduce the stabilizing effect of rotation. It is also shown that the boundary of a steady convection cell is distorted by the rotation in such a way that the wavelength of the cell measured along the distorted boundary is equal to the wavelength of the non-rotating cell. This conservation of cellular wavelength is traced to the constancy of horizontal vorticity in the rotating and non-rotating systems. In the finite-amplitude investigation the analysis, which is pivoted about the linear stability problem, indicates that the fluid can become unstable to finite-amplitude disturbances before it becomes unstable to infinitesimal perturbations. The finite-amplitude motions generate a non-linear vorticity which tends to counteract the vorticity generated by the imposed constraint of rotation. Under experimental conditions the two fluids, mercury and air, which are considered in this paper, will not exhibit this finite amplitude instability. However, a fluid with a sufficiently small Prandtl number will become unstable to finite-amplitude perturbations. The special role of viscosity as an energy releasing mechanism in this problem and in the Orr-Sommerfeld problem suggests that the occurrence of a finite-amplitude instability depends on this dual role of viscosity (i.e. as an energy releasing mechanism as well as the more familiar dissipative mechanism). The relative stability criterion developed by Malkus & Veronis (1958) is used to determine the preferred type of cellular motions which can occur in the fluid. This preferred motion is a function of the Prandtl number and the Taylor number. In the case of air it is shown that overstable square cells become preferred in finite amplitude, even though steady convective motions occur at a lower Rayleigh number.

Introduction

The columnar structure in figure 1 represents the manner in which the boundary of a hexagonal convection cell in a fluid is distorted by an imposed uniform rotation of the entire system. The distortion plays an important role in the determination of the finite amplitude effects in the convecting fluid. We shall study this geometry of cellular convection as part of a more general investigation into the nature of cellular convection in a rotating fluid.

The constraint of rotation is, of course, only one of a large number of externally imposed constraints to which a fluid may be subjected. Yet a detailed knowledge of the constraining effect of rotation and of the finite-amplitude behaviour of the rotating fluid may provide an insight into the mechanism of a broad class of problems in which the system is constrained externally.

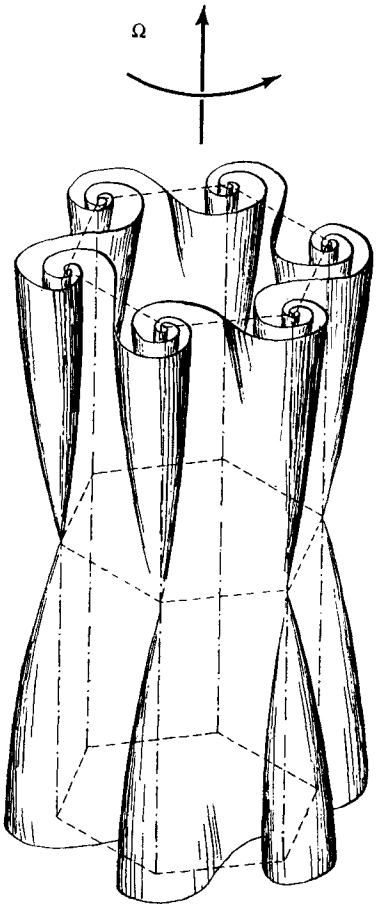

FIGURE 1. A perspective sketch of a hexagonal convection cell as it is distorted by an imposed rotation of the fluid.

As a starting-point for this discussion, we have available several previous studies. The stability problem has been investigated theoretically by Chandrasekhar (1953) and by Nakagawa & Frenzen (1955) (hereafter these papers will be referred to as II and III respectively), and experimentally by Nakagawa & Frenzen (1955) and by Fultz & Nakagawa (1955). Finite amplitude cellular convection in a non-rotating fluid has been considered by Malkus & Veronis (1958) (hereafter referred to as I). The questions which we may hope to answer in this paper may be posed more clearly in the light of these investigations.

When a horizontally infinite layer of fluid is heated uniformly from below and cooled from above, the system is stable to infinitesimal disturbances for values of

the Rayleigh number λ below a critical value λ_0. Here, $\lambda = \alpha g \beta_m d^4/\kappa\nu$, where g is the gravitational acceleration; α, ν and κ are respectively the coefficients of expansion, kinematic viscosity and thermometric diffusivity of the fluid; d is the depth of the fluid; and $\beta_m = (T_H - T_C)/d$, where T_H and T_C are respectively the temperatures at the bottom and top surfaces of the layer. When $\lambda \geqslant \lambda_0$, the fluid is unstable and convective motions occur leading to a distortion of the mean (horizontally averaged) temperature field. Experimentally, convection is observed to set in as a fairly regular cellular pattern in the horizontal.

The specific value of λ_0 depends on the boundary conditions. In the non-rotating system, λ_0 is constant for a particular set of boundary conditions. In the rotating fluid, the specific value of the critical Rayleigh number depends on the value of the Taylor number $\mathscr{T}^2 = 4\Omega^2 d^4/\nu^2$ (where Ω is the uniform angular velocity of the system) and on the value of the Prandtl number $\sigma\,(\equiv \nu/\kappa)$. The general effect of the rotation is to increase λ_0 and to decrease the horizontal scale of the cells. For large, but experimentally realizable, values of $\mathscr{T}^2$, the value of λ_0 may be as high as 10^5 times the critical Rayleigh number corresponding to the non-rotating system. It has been noted both experimentally and theoretically (cf. II and III) that for a range of values of the parameters σ and $\mathscr{T}^2$, instability can arise as a time-periodic motion. In the greater part of the range, this so-called 'overstability' occurs before steady convective instability.

A number of interesting questions arise from the study of the stability problem. Although the horizontal scale of the cells diminishes with rotation, what similarities exist between the motions of the constrained and unconstrained systems? What physical mechanism causes overstability to occur and to be preferred to steady convective instability? Is it possible that the initial instability occurs as convection, but that overstability can enter and become the preferred state of motion in finite amplitude? Is the reverse possible?

As we have noted, the constraining effect of rotation manifests itself principally by making the system more stable, i.e. by increasing the value of λ_0. That the rotating system will behave differently from the non-rotating fluid in finite amplitude is indicated by the fact that viscosity plays a dual role here. In addition to its more familiar role of dissipating the kinetic energy of the fluid, the viscosity serves also as the energy releasing mechanism. The fluid particles are constrained by the rotation to move in the direction of the rotation vector $\boldsymbol{\Omega}$. Only through the presence of viscosity do they find a means for achieving cross-isobar flow through which potential energy is released. This dual role of viscosity as a function of rotation is no more evident than it is in the fact that (cf. II) for sufficiently high rotation rates, a fluid confined by rigid boundaries becomes unstable for a value of λ_0 lower than the λ_0 corresponding to a fluid confined by free boundaries where viscous effects are smaller. In the non-rotating case, the free boundary conditions have always led to lower λ_0.

As a further guide to the finite amplitude study we turn to the analysis of finite amplitude convection in the non-rotating system (I).

After the fluid has become unstable, the convective motions lead to a distortion of the mean temperature profile. When the Prandtl number is large, the amount of heat which is transported vertically by convection is determined principally by

this distortion of the mean temperature field. For $\sigma < 1$, the self-distortion of the cellular structure plays an important role in the determination of the vertical heat transport. Since the constraint of rotation adds to the distortion of the cellular structure, we can anticipate that in the present study the self-distortion of the cell will be more important in determining the heat transport.

All close-packed cellular patterns (rectangles, hexagons, triangles and two-dimensional rolls) are mathematically possible in finite amplitude. A relative stability criterion was developed in I to determine which of the many possible steady solutions will actually be realized. When the system has vertical symmetry and free boundaries, square cells are the preferred pattern for $\sigma > 0{\cdot}8$, and limiting rectangles (one side becomes infinitely long) for $\sigma \leqslant 0{\cdot}8$. When a vertical asymmetry is present (e.g. free upper boundary, rigid lower boundary), hexagonal cells are preferred when λ exceeds λ_0 by a small amount.

The qualitative results relating to symmetrical and asymmetrical systems ought not to be altered by the presence of rotation. However, is the preferred cellular pattern for a symmetric system a function of the rotation rate? What effect has overstability on the geometrical pattern of the flow?

More general questions are the following. What is the mechanism through which the constraint manifests itself in the flow? Does the fluid organize itself so as to minimize the effects of the externally imposed constraint? Indeed, is it possible for the fluid to generate its own 'constraint' to offset the imposed one?

1. Equations and boundary conditions

This problem is one of a large class of convection problems in which the Boussinesq (1903) approximation may be applied. The density is considered to be constant everywhere in the equations except in the buoyant force term. The equations for the local conservation of heat, momentum and mass are then

$$\frac{\partial \tilde{T}}{\partial t} - \kappa \nabla^2 \tilde{T} = -\mathbf{v} \cdot \nabla \tilde{T}, \tag{1.1}$$

$$\frac{\partial \mathbf{v}}{\partial t} + \mathbf{v} \cdot \nabla \mathbf{v} + 2\Omega \mathbf{k} \times \mathbf{v} = -\frac{1}{\rho_m} \nabla p + \gamma \tilde{T} \mathbf{k} + \nu \nabla^2 \mathbf{v}, \tag{1.2}$$

$$\nabla \cdot \mathbf{v} = 0, \tag{1.3}$$

where the equation of state

$$\rho = \rho_m (1 - \alpha \tilde{T}) \tag{1.4}$$

has been used in the buoyancy term. In these equations $\tilde{T}$ is the deviation of the temperature from its mean value, ρ_m is the mean density of fluid, $\mathbf{v}$ is the three-dimensional velocity field (u, v, w) in the directions (x, y, z) respectively, t is the time, $\mathbf{k}$ is the unit vector in the vertical (z) direction, ∇^2 is the three-dimensional Laplacean operator, $p = \tilde{p} - gz$, where $\tilde{p}$ is the pressure, $\gamma = \alpha g$, and the remaining terms have been defined in the introduction.

We consider an ensemble of systems with the given fixed boundary conditions. These systems will have arbitrary phases in time and horizontal space. An ensemble average denotes an average over these arbitrary phases, and, consequently, $\tilde{T}$ can be subdivided into a portion which is a function only of the vertical co-ordinate and a fluctuation which is a function of x, y, z and t.

Let
$$\tilde{T} = T(z) + T(x, y, z, t), \tag{1.5}$$
where $T(z)$ denotes the ensemble-average temperature. Thus, letting a bar over a quantity denote the ensemble-average, we have
$$\overline{\tilde{T}} = T(z), \quad \overline{T(x, y, z, t)} = 0.$$
The substitution of (1.5) into (1.1) yields
$$\frac{\partial T}{\partial t} - \kappa \frac{\partial^2 T(z)}{\partial z^2} - \kappa \nabla^2 T = \beta w - \mathbf{v} . \nabla T, \tag{1.6}$$
where $\beta = -\partial T(z)/\partial z$ is the negative vertical gradient of mean temperature. By taking an ensemble-average of (1.6), one gets
$$-\kappa \frac{\partial^2 T(z)}{\partial z^2} = -\frac{\partial}{\partial z}(\overline{wT}), \tag{1.7}$$
which can be integrated once to yield
$$\kappa\beta + \overline{wT} = H, \tag{1.8}$$
where H is the vertical heat flux in the fluid and is constant for an ensemble of systems with given fixed boundary conditions. Thus, taking a vertical average $\left(= \frac{1}{d}\int_0^d H\, dz\right)$ yields
$$\kappa\beta_m + \{wT\}_m = H, \tag{1.9}$$
where $\{\}_m$ denotes both an ensemble and a vertical average.

From (1.8) and (1.9), we have
$$\frac{\beta}{\beta_m} = 1 + \frac{\{wT\}_m - \overline{wT}}{\kappa\beta_m}. \tag{1.10}$$
Equation (1.10) provides a means for determining the distortion of the mean temperature field from the values of the fluctuation quantities w and T.

Substituting (1.7) into (1.6) and making use of (1.10), we have
$$\frac{\partial T}{\partial t} - \kappa \nabla^2 T - \beta_m w = \frac{\{wT\}_m - \overline{wT}}{\kappa} - h, \tag{1.11}$$
where $h = \mathbf{v} . \nabla T - \partial(\overline{wT})/\partial z$ represents the zero-average heat advection terms.

The pressure p (relative to hydrostatic pressure) can be eliminated from (1.2) to yield
$$\frac{\partial}{\partial t}\nabla^2 w + 2\Omega \frac{\partial \zeta}{\partial z} - \gamma \nabla_1^2 T = \nu \nabla^4 w + L, \tag{1.12}$$
where $$L = \frac{\partial}{\partial z}\left[\frac{\partial}{\partial x}(\mathbf{v} . \nabla u) + \frac{\partial}{\partial y}(\mathbf{v} . \nabla v)\right] - \nabla_1^2(\mathbf{v} . \nabla w), \quad \nabla_1^2 = \frac{\partial^2}{\partial x^2} + \frac{\partial^2}{\partial y^2},$$
and $\zeta = \partial v/\partial x - \partial u/\partial y$ is the vertical component of vorticity. From the first two equations of (1.2), an additional relation between ζ and w can be derived:
$$\frac{\partial \zeta}{\partial t} - \nu \nabla^2 \zeta - 2\Omega \frac{\partial w}{\partial z} = -Z, \tag{1.13}$$
where $Z = \frac{\partial}{\partial x}(\mathbf{v} . \nabla v) - \frac{\partial}{\partial y}(\mathbf{v} . \nabla u)$. The terms L and Z appearing in (1.12) and (1.13) are both zero-average non-linear terms.

Because the subsequent analysis will be based on an expansion of each of the variables, it is convenient to work with the equations in dimensionless form. Thus, letting $\mathbf{v} = \nu\mathbf{v}'/d$, $\mathbf{r} = d\mathbf{r}'$, $\nabla = d^{-1}\nabla'$, $T = \kappa\nu T'/\gamma d^3$, $t = d^2\tau/\kappa$, $\sigma = \nu/\kappa$, one has

$$\left(\frac{\partial}{\partial\tau} - \nabla^2\right) T - \sigma\lambda w = \sigma^2[\{wT\}_m - \overline{wT}]\, w - \sigma h, \tag{1.11 bis}$$

$$\left(\frac{1}{\sigma}\frac{\partial}{\partial\tau} - \nabla^2\right) \nabla^2 w + \mathscr{T}\frac{\partial\zeta}{\partial z} - \frac{1}{\sigma}\nabla_1^2 T = L, \tag{1.12 bis}$$

$$\left(\frac{1}{\sigma}\frac{\partial}{\partial\tau} - \nabla^2\right) \zeta - \mathscr{T}\frac{\partial w}{\partial z} = -Z, \tag{1.13 bis}$$

where the primes have been dropped from the variables. *Throughout the remainder of the work, unprimed quantities will denote dimensionless variables unless otherwise noted.* In these equations $\mathscr{T} = 2\Omega d^2/\nu$ is the square root of the Taylor number.

The analysis will be pivoted about the linear stability solution and it is therefore convenient to eliminate all but one of the variables in the linear operators. Elimination of T and ζ from the left-hand sides of (1.11), (1.12) and (1.13) gives

$$\begin{aligned}\left(\frac{1}{\sigma}\frac{\partial}{\partial\tau} - \nabla^2\right)^2 \left(\frac{\partial}{\partial\tau} - \nabla^2\right) \nabla^2 w + \mathscr{T}^2\left(\frac{\partial}{\partial\tau} - \nabla^2\right) \frac{\partial^2 w}{\partial z^2} - \left(\frac{1}{\sigma}\frac{\partial}{\partial\tau} - \nabla^2\right) \lambda\nabla_1^2 w \\ = \sigma\left(\frac{1}{\sigma}\frac{\partial}{\partial\tau} - \nabla^2\right) [\{wT\}_m - \overline{wT}]\, \nabla_1^2 w \\ + \mathscr{T}\left(\frac{\partial}{\partial\tau} - \nabla^2\right) \frac{\partial Z}{\partial z} - \left(\frac{1}{\sigma}\frac{\partial}{\partial\tau} - \nabla^2\right) \nabla_1^2 h + \left(\frac{\partial}{\partial\tau} - \nabla^2\right) \left(\frac{1}{\sigma}\frac{\partial}{\partial\tau} - \nabla^2\right) L.\end{aligned} \tag{1.14}$$

Equations (1.3), (1.11), (1.13) and (1.14) are the basic equations of our analysis. A perturbation method similar to that employed in I is used to derive approximate solutions.

Let

$$\left.\begin{aligned} w &= \epsilon w_0 + \epsilon^2 w_1 + \epsilon^3 w_2 + \epsilon^4 w_3 + \ldots, \\ T &= \epsilon T_0 + \epsilon^2 T_1 + \epsilon^3 T_2 + \epsilon^4 T_3 + \ldots, \\ u &= \epsilon u_0 + \epsilon^2 u_1 + \epsilon^3 u_2 + \epsilon^4 u_3 + \ldots, \\ v &= \epsilon v_0 + \epsilon^2 v_1 + \epsilon^3 v_2 + \epsilon^4 v_3 + \ldots. \end{aligned}\right\} \tag{1.15}$$

The parameter ϵ must be identified with the amplitude. Since the value of λ determines the amplitude, a relation between λ and ϵ must also be deduced. As in I, λ is also expanded in terms of ϵ: thus

$$\lambda = \lambda_0 + \epsilon\lambda_1 + \epsilon^2\lambda_2 + \epsilon^3\lambda_3 + \epsilon^4\lambda_4 + \ldots, \tag{1.16}$$

where the λ_i are to be determined.

If the expansions (1.15) and (1.16) are introduced into equations (1.3), (1.11), (1.13) and (1.14), and if the coefficients of each order of ϵ are equated, a series of equations is derived involving the variables w_i, T_i, u_i and v_i. We shall postpone writing the resulting relations explicitly until we come to the specific sections on finite-amplitude steady convection and finite-amplitude overstability.

An additional equation, which we shall find useful, results from multiplying (1.2) by $\mathbf{v}$ and averaging. This yields in non-dimensional form

$$\sigma\{\mathbf{v}\,.\,\nabla^2\mathbf{v}\}_m + \{wT\}_m = \frac{\partial}{\partial\tau}\{\tfrac{1}{2}\mathbf{v}\,.\,\mathbf{v}\}_m. \tag{1.17}$$

Equation (1.17) asserts that the rate of change of kinetic energy is equal to the rate of release of potential energy minus the rate of viscous dissipation of kinetic energy (the first term on the left is negative definite). In our problems the right-hand side will vanish.

Boundary conditions

If the boundary at the top or the bottom surface is considered 'free', the conditions on the velocities are

$$w = 0, \quad \frac{\partial v}{\partial z} = \frac{\partial u}{\partial z} = \frac{\partial^2 w}{\partial z^2} = 0 \tag{1.18}$$

at the boundary. At rigid boundaries, the conditions are

$$w = 0, \quad u = v = \frac{\partial w}{\partial z} = 0. \tag{1.19}$$

In the present investigation both boundaries are considered 'free'. Although this is an idealization, nevertheless it permits one to determine most of the qualitative features of the flow. The rigid boundary conditions lead to such a formidable computational problem (cf. I) that the present method of solution is practically useless.

Thermally, the boundaries are considered perfect conductors. For air or water, most metal boundaries will by comparison be nearly perfect conductors. For a fluid such as mercury, silver or copper boundaries approximate the ideal boundary material. Hence, at the bounding surfaces, we take

$$T = 0. \tag{1.20}$$

If we evaluate the basic equations (1.11) and (1.12) at a free boundary where $T = 0$, then (1.12) becomes

$$\frac{\partial^4 w}{\partial z^4} = 0. \tag{1.21}$$

2. Stability problem

The equations for the stability problem can be determined either by substituting the expansions (1.15) and (1.16) in equations (1.3), (1.11), (1.13) and (1.14), and then taking only the first-order terms in ϵ, or alternatively by simply neglecting all the non-linear terms in the equations. In either case, the equations are

$$\left(\frac{\partial}{\partial \tau} - \nabla^2\right) T_0 - \sigma \lambda_0 w_0 = 0, \tag{2.1a}$$

$$\left(\frac{1}{\sigma}\frac{\partial}{\partial \tau} - \nabla^2\right) \zeta_0 - \mathscr{T}\frac{\partial w_0}{\partial z} = 0, \tag{2.1b}$$

$$\left(\frac{1}{\sigma}\frac{\partial}{\partial \tau} - \nabla^2\right)^2 \left(\frac{\partial}{\partial \tau} - \nabla^2\right) \nabla^2 w_0 + \mathscr{T}^2 \left(\frac{\partial}{\partial \tau} - \nabla^2\right) \frac{\partial^2 w_0}{\partial z^2} - \left(\frac{1}{\sigma}\frac{\partial}{\partial \tau} - \nabla^2\right) \lambda_0 \nabla_1^2 w_0 = 0, \tag{2.1c}$$

$$\frac{\partial u_0}{\partial x} + \frac{\partial v_0}{\partial y} + \frac{\partial w_0}{\partial z} = 0, \tag{2.1d}$$

where the subscript zero has been included in order to identify the variables with the stability problem.

Experimentally, convection is seen to occur as a close-packed cellular regime. This indicates that a useful analytical approach to the stability problem is to assume separability of horizontal and vertical dependence and to assume a periodic horizontal structure. These two simplifications are written as

$$w_0 = e^{p_0\tau} f(x,y)\, g(z), \quad \nabla_1^2 f(x,y) = -\alpha^2 \pi^2 f(x,y), \tag{2.2}$$

where α is the effective horizontal wave number and the time dependence is chosen as $e^{p_0\tau}$ as is customary in linear stability theory.

The stability problem can now be solved immediately (cf. II) since the free boundary conditions on w_0 are satisfied by $g(z) = \sin n\pi z$. If

$$w_0 = e^{p_0\tau} f(x,y) \sin n\pi z \tag{2.3}$$

is substituted into (2.1*c*), it is found that

$$(\alpha^2+n^2)[p_0+\pi^2(\alpha^2+n^2)][p_0/\sigma+\pi^2(\alpha^2+n^2)]^2+\mathscr{T}^2 n^2[p_0+\pi^2(\alpha^2+n^2)] - \alpha^2\lambda_0[p_0/\sigma+\pi^2(\alpha^2+n^2)] = 0,$$

hence, on rearrangement,

$$p_0^3+(2\sigma+1)\pi^2(\alpha^2+n^2)p_0^2+[\pi^4(\alpha^2+n^2)^2(\sigma^2+2\sigma)+(\mathscr{T}^2 n^2\sigma-\alpha^2\lambda_0)\sigma/(\alpha^2+n^2)]p_0 + \sigma^2\pi^6(\alpha^2+n^2)^3+\sigma^2\pi^2(\mathscr{T}^2 n^2-\alpha^2\lambda_0) = 0. \tag{2.4}$$

A. *Steady convective instability*

If p_0 is real, marginal instability occurs when $p_0 = 0$, i.e. when

$$\frac{\lambda_0}{\pi^4} = \frac{(\alpha^2+n^2)^3+\mathscr{T}_1^2 n^2}{\alpha^2}, \tag{2.5}$$

where $\mathscr{T}_1^2 = \mathscr{T}^2/\pi^4$. From

$$\frac{\partial\lambda_0}{\partial\alpha^2} = 2\alpha^6+3\alpha^4 n^2-n^6-\mathscr{T}_1^2 n^2 = 0, \tag{2.6}$$

we can find that value of α^2, as a function of $\mathscr{T}_1^2$ and n^2, which minimizes λ_0/π^4.

We note immediately from (2.6) and (2.5) that $\lambda_0/\pi^4 \to 3(\frac{1}{2}\mathscr{T}_1^2 n^2)^{\frac{2}{3}}$ and $\alpha^2 \to (\frac{1}{2}\mathscr{T}_1^2 n^2)^{\frac{1}{3}}$ as $\mathscr{T}_1^2 \to \infty$. Thus, as the Taylor number increases, λ_0 increases and the cellular diameter decreases. It is evident also that λ_0/π^4 attains its minimum value when $n = 1$ (neglecting the trivial case $n = 0$ when there is no motion). A curve of λ_0/π^4 *vs* $\mathscr{T}_1^2$ is plotted in figure 5.

Since $\mathscr{T}_1^2$ is inversely proportional to the square of the viscosity, the asymptotic expression, $\lambda_0/\pi^4 \to 3(\frac{1}{2}\mathscr{T}_1^2 n^2)^{\frac{2}{3}}$ asserts that both the critical Rayleigh number and the actual critical temperature difference $T_H - T_C$ decreases with increasing viscosity. This destabilizing effect of viscosity plays an important role in the finite-amplitude behaviour of the fluid, and we shall refer to it again later.

The motions associated with the point of instability depend on the particular cellular pattern which is postulated. These motions will be presented here in some detail because a knowledge of them provides some insight into the finite-amplitude behaviour of the fluid.

B. *Geometry of the fluid motion*

The possible horizontal patterns for close-packed cells are limited to two-dimensional rolls, hexagons, triangles and rectangles. Though the first of these cannot occur in an experimental investigation, it represents the simplest type of motion and will be discussed first.

Rolls. Let w_0 be independent of the y-co-ordinate. The solution (2.2) which satisfies the symmetry condition $\partial w_0/\partial x = 0$ at the walls of the cell is

$$w_0 = 2\cos\pi\alpha x \sin\pi z, \tag{2.7}$$

where, for reasons which will appear later, w_0 has been normalized, i.e. $\{w_0^2\}_m = 1$. (The normalization does not affect the present discussion.)

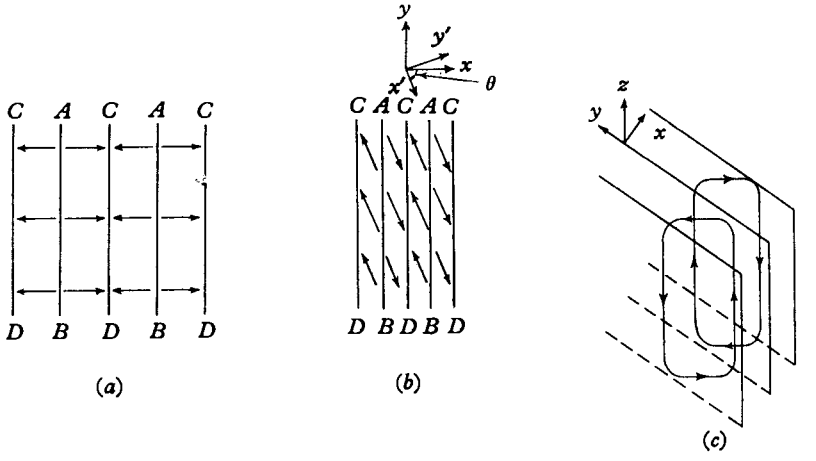

FIGURE 2. (*a*) A top view of two-dimensional rolls in a non-rotating fluid. The arrows indicate the direction of motion of the fluid. (*b*) The same in a system rotating counter-clockwise. (*c*) A perspective view of fluid particle motions in a role when the fluid is rotated.

From equations (2.1), the temperature T_0 and the velocity components u_0, v_0 are

$$T_0 = \frac{2\sigma\lambda_0}{\pi^2(\alpha^2+1)}\cos\pi\alpha x\sin\pi z, \quad u_0 = -\frac{2}{\alpha}\sin\pi\alpha x\cos\pi z,$$
$$v_0 = \frac{2\mathscr{T}_1}{\alpha(\alpha^2+1)}\sin\pi\alpha x\cos\pi z. \tag{2.8}$$

When $\mathscr{T}_1 = 0$, we have $v_0 = 0$ and the fluid motion is in the x-direction only. In figure 2*a* a view of the top of a non-rotating fluid layer is shown. The fluid has maximum upward velocity along lines AB and maximum downward velocity along lines CD.

When the system is rotated, the coriolis force introduces a velocity component parallel to the isobars (isotherms in this case), i.e. in the y-direction. Therefore, the streamlines are oriented at an oblique angle to the y-axis (figure 2*b*).

The wave-number α of the cell is a function of $\mathscr{T}_1^2$ as given by (2.6). The wave number corresponding to the oblique cell, i.e. in the direction of the orientation of

the cell, can be computed from (2.8). Let θ be the angle from the x-axis to the streamline path as indicated in figure 2*b*. Then

$$\theta = \tan^{-1}\left(\frac{v_0}{u_0}\right) = -\tan^{-1}\left(\frac{\mathscr{T}_1}{\alpha^2+1}\right). \tag{2.9}$$

The square of the wave-number of the oblique cell is given by

$$\alpha^2\cos^2\theta = \frac{\alpha^2(\alpha^2+1)^2}{\mathscr{T}_1^2+(\alpha^2+1)^2}. \tag{2.10}$$

With (2.6), this expression reduces to

$$\alpha^2\cos^2\theta = \alpha^2(1/2\alpha^2) = \tfrac{1}{2}. \tag{2.11}$$

In other words, although the wavelength of the cell decreases with rotation, the wavelength of the cell measured in the direction of the orientation of the cell is the same as in the non-rotating case.

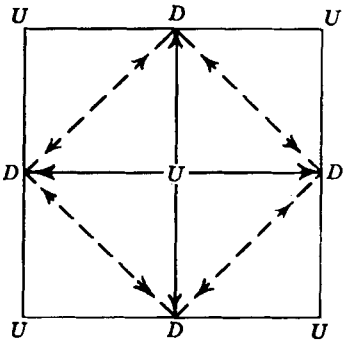

FIGURE 3*a*. A top view of square cells in a non-rotating fluid. Points marked U are points of maximum upward velocity; those marked D are points of maximum downward velocity. The region within the dotted lines would be seen as a cell in an experiment.

Square cells. From the analysis of the non-rotating system we anticipate that square cells will be the preferred form for a system with vertical symmetry. Paralleling the argument for rolls, we can write

$$\left.\begin{aligned} w_0 &= 2\sqrt{2}\cos\frac{\pi\alpha x}{\sqrt{2}}\cos\frac{\pi\alpha y}{\sqrt{2}}\sin\pi z, \quad T_0 = \frac{\sigma\lambda_0}{\pi^2(\alpha^2+1)}w_0, \\ u_0 &= -\left[\frac{2\mathscr{T}_1}{\alpha(\alpha^2+1)}\cos\frac{\pi\alpha x}{\sqrt{2}}\sin\frac{\pi\alpha y}{\sqrt{2}}+\frac{2}{\alpha}\sin\frac{\pi\alpha x}{\sqrt{2}}\cos\frac{\pi\alpha y}{\sqrt{2}}\right]\cos\pi z, \\ v_0 &= \left[-\frac{2}{\alpha}\cos\frac{\pi\alpha x}{\sqrt{2}}\sin\frac{\pi\alpha y}{\sqrt{2}}+\frac{2\mathscr{T}_1}{\alpha(\alpha^2+1)}\sin\frac{\pi\alpha x}{\sqrt{2}}\cos\frac{\pi\alpha y}{\sqrt{2}}\right]\cos\pi z. \end{aligned}\right\} \tag{2.12}$$

When $\mathscr{T}_1 = 0$, both the horizontal and the vertical motions form a square pattern. A top view of the fluid is illustrated in figure 3*a*, where U and D define points of maximum upward and downward motions respectively. The cell is shown with fluid rising in the centre, but the pattern can equally as well be displaced by a half wavelength in the x- or y-direction to yield a cell with sinking at the centre. In actuality the region within the dotted lines is what one would see as a cell in an experiment.

When $\mathscr{T}_1 > 0$, the coriolis force causes the fluid to turn as it moves toward or from the centre so that part of the flow is parallel to the isobars. The spiral curves in figure 3*b* correspond to the straight lines shown in figure 3*a*. As the spiral crosses the x- and y-axes, it coincides with the inverse logarithmic spiral $r = \alpha^{-1}\exp\{\mathscr{T}_1\theta/(\alpha^2+1)\}$ (in polar co-ordinates r, θ), but the regions intermediate to the axes, it deviates from the logarithmic spiral. (The actual spiral is not equiangular, i.e. it does not cross all radial lines with the same angle at each traversal. The logarithmic spiral was used to construct the figure and to compute the half wavelength along the path.) By computing the length of the spiral, one can derive expression (2.11) for the horizontal 'wave-number' along the spiral. The wavelength measured along the distorted cellular boundary is again equal to that of the non-rotating case.

Figure 3*c* is a perspective sketch of a complete trajectory of a particle which travels from the centre of the cell to the edge and back again. The particle spirals upward and clockwise (for counterclockwise Ω) from the centre of the cell, crosses to the corner near the top of the cell and spirals downward and counterclockwise. Halfway down it reverses its direction of rotation, spirals downward and clockwise crosses back toward the middle of the cell, and begins a counterclockwise upward motion toward the centre.

The reversal of rotation as a particle crosses the middle plane is due to the fact that at this point the horizontal divergence of the fluid changes sign. As the fluid moves outward, it is deflected to the right by the coriolis force and spirals in a clockwise manner. Converging fluid spirals counterclockwise when deflected to the right.

The square cell shown in the diagram corresponds to the basic geometry of the vertical velocity. The actual cell is distorted by the rotation and is not reproduced here.

Hexagonal cells. The preferred pattern for the vertical velocity is the hexagonal pattern when the boundary conditions provide a vertical asymmetry. Since most experimental observations of cells are made when the upper surface is free, hexagonal cells will ordinarily occur.

The discussion parallels that for square cells. The analytical form as proposed by Christopherson (1940) is

$$w_0 = \frac{2}{\sqrt{3}}\left\{2\cos\frac{2\pi x}{\sqrt{3}L}\cos\frac{2\pi y}{3L} + \cos\frac{4\pi y}{3L}\right\}\sin\pi z, \tag{2.13a}$$

where $L = 4/(3\alpha)$ is the length of one side of the regular hexagon. The remaining variables have the form

$$\left.\begin{aligned} T_0 &= \frac{\sigma\lambda_0}{\pi^2(\alpha^2+1)}w_0, \\ u_0 &= -\left[\frac{3L}{2}\sin\frac{2\pi x}{\sqrt{3}L}\cos\frac{2\pi y}{3L} + \frac{\sqrt{3}L\mathscr{T}_1}{2(\alpha^2+1)}\left(\cos\frac{2\pi x}{\sqrt{3}L}\sin\frac{2\pi y}{3L} + \sin\frac{4\pi y}{3L}\right)\right]\cos\pi z, \\ v_0 &= \left[\frac{3L\mathscr{T}_1}{2(\alpha^2+1)}\sin\frac{2\pi x}{\sqrt{3}L}\cos\frac{2\pi y}{3L} - \frac{\sqrt{3}L}{2}\left(\cos\frac{2\pi x}{\sqrt{3}L}\sin\frac{2\pi y}{3L} + \sin\frac{4\pi y}{3L}\right)\right]\cos\pi z. \end{aligned}\right\} \tag{2.13b}$$

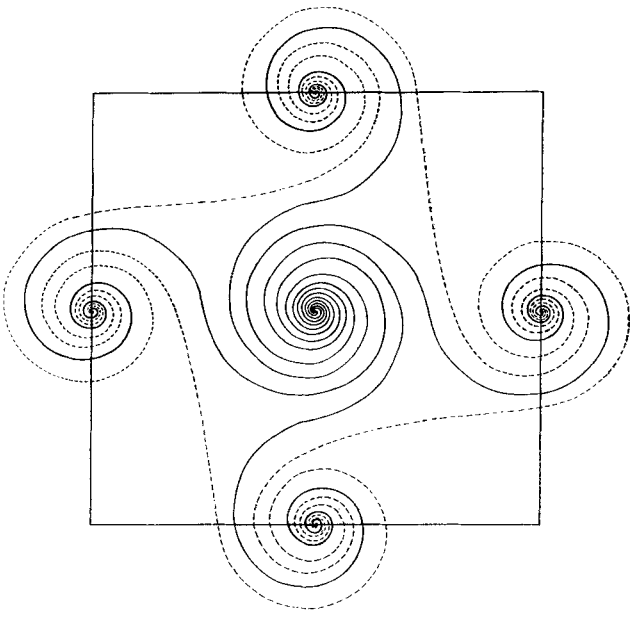

FIGURE 3*b*. A square cell in a rotating fluid. The particle motions from the centre outward follow the spiral curves. The dashed curves form the boundary of the square cell.

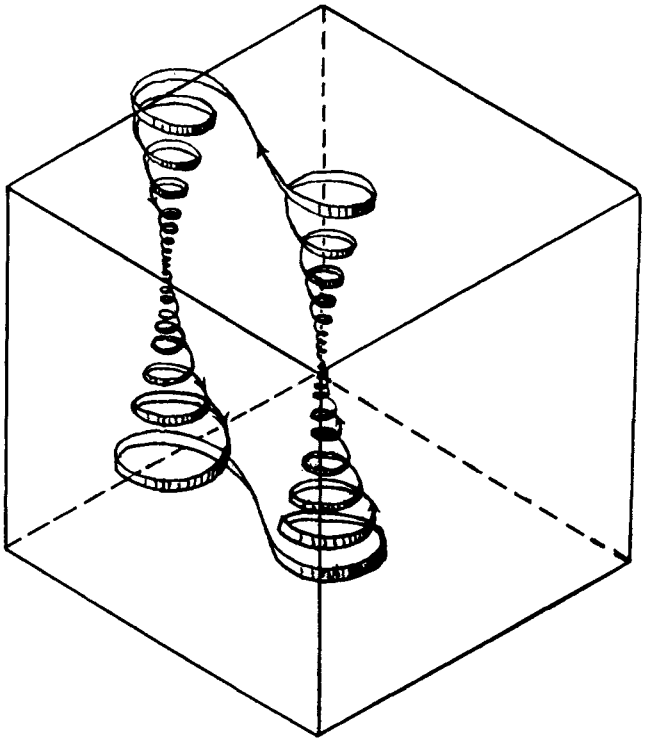

FIGURE 3*c*. A perspective sketch of a fluid particle motion in the square cell.

Figure 4*a* illustrates the particle motion at the top of a non-rotating-cell. Figure 4*b* is a top view of a rotating cell and of the six adjacent cells. The dashed spirals form the upper boundary of the centre cell. Each centre is surrounded by six corners and each corner receives fluid from the three adjacent centres.

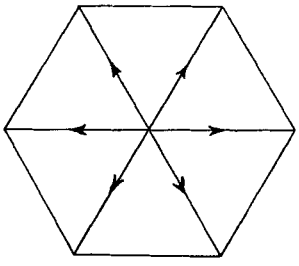

FIGURE 4*a*. Top view of a non-rotating hexagonal cell. The fluid rises in the centre and spreads outward to the six corners where it descends.

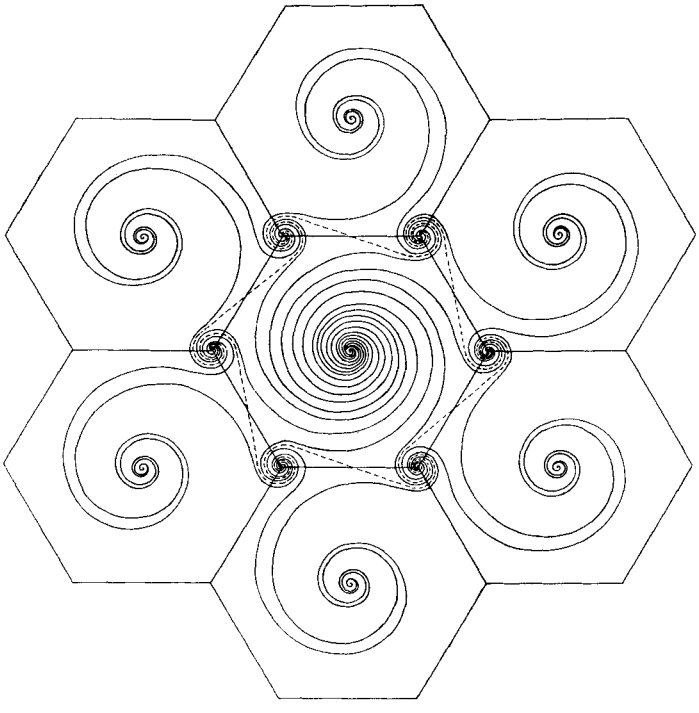

FIGURE 4*b*. A top view of seven rotating hexagonal cells. The fluid particles follow spiral paths from the centre toward the corners. The dashed lines form the boundaries of the centre cell.

A perspective sketch of a fluid particle path in three dimensions is shown in figure 4*c*. Figure 1 illustrates the manner in which the cell is distorted by the rotation.

The effective wave-number of the non-rotating cell is again equal to the wave-number measured along the spiral curve.

The three cases discussed here indicate that the wave-number measured along the curved path is invariant. It is clear that such an invariance must be intimately coupled with a physical property of the fluid which is unaffected by the imposed constraint. The one property of the fluid which is not affected by a rotation about a vertical axis is the horizontal vorticity. We shall show here how the constancy of horizontal vorticity preserves the wave-number measured in the direction of flow for the simplest type of motion, viz. that of rolls.

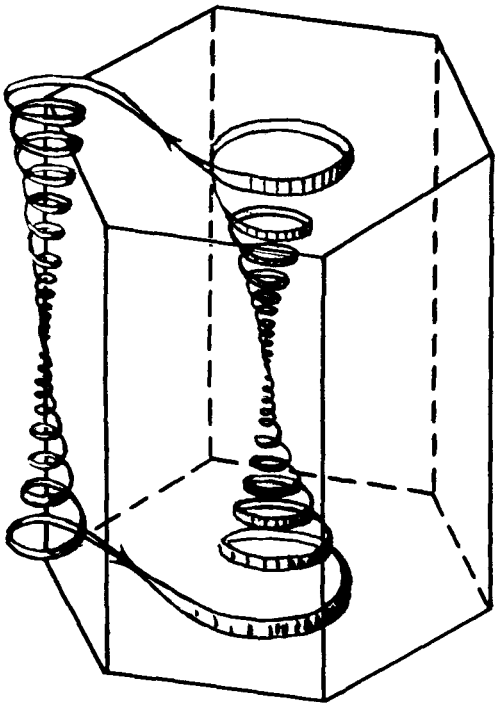

FIGURE 4c. A perspective sketch of a fluid particle path which passes through the centre of the cell.

Consider a rotation of the horizontal co-ordinates so that the x'-direction is measured along the direction of flow (figure 2*b*). Then the horizontal vorticity about the y-axis is given by $\partial u'/\partial z - \partial w/\partial x'$, where the primes correspond to a measure of the quantities along the new axes. Since the horizontal vorticity is constant, we have

$$\left\{\left(\frac{\partial u'}{\partial z}-\frac{\partial w}{\partial x'}\right)^2\right\}_m = \left\{\left(\frac{\partial u}{\partial z}-\frac{\partial w}{\partial x}\right)^2\right\}_m = \text{const.}, \tag{2.14}$$

where the middle expression corresponds to the non-rotating system, i.e. when x' is parallel to x. From the equation of continuity, we have

$$\frac{\partial u'}{\partial x'}+\frac{\partial w}{\partial z}=0, \quad \frac{\partial u}{\partial x}+\frac{\partial w}{\partial z}=0. \tag{2.15}$$

Since w is normalized and since the z-distance is fixed, equation (2.15) yields a relation between the wave-number measured in the x (or x') direction and the

amplitude of u (or u'). From (2.14) we then note that the wave-number must be the same in the two systems. When the vertical velocity is normalized the amplitudes of the horizontal velocities are equal.

C. *Overstability*

Though p_0 must be real in the non-rotating system, p_0 may be complex when $\mathscr{T}^2 > 0$. The coefficients of (2.4) are real; therefore, in general p_0 will have one real and two complex conjugate roots. These can be written in the form

$$(p_0-p')\,(p_0-p_r-ip_i)\,(p_0-p_r+ip_i) = 0,$$

or
$$p_0^3-(p'+2p_r)\,p_0^2+(2p_rp'+p_i^2+p_r^2)\,p_0-p'(p_i^2+p_r^2) = 0,$$

where p', p_i and p_r are real.

For marginal stability $p_r = 0$, and

$$p_0^3-p'p_0^2+p_i^2p_0-p'p_i^2 = 0. \tag{2.16}$$

Hence, for marginal stability, the product of the coefficients of p_0^2 and p_0 must equal the coefficient of p_0^0. By (2.4) this condition becomes

$$\frac{\lambda_0}{\pi^4} = 2(\sigma+1)\left[\frac{(\alpha^2+n^2)^3+\dfrac{\sigma^2}{(\sigma+1)^2}n^2\mathscr{T}_1^2}{\alpha^2}\right], \tag{2.17}$$

which has a minimum when $\partial\lambda_0/\partial\alpha^2 = 0$, i.e. when

$$2\alpha^6+3\alpha^4n^2 = n^6+\frac{\sigma^2}{(\sigma+1)^2}n^2\mathscr{T}_1^2. \tag{2.18}$$

Thus $\alpha^2 \to 2^{-\frac{1}{3}}[\sigma n\mathscr{T}_1/(\sigma+1)]^{\frac{2}{3}}$ and $\lambda_0/\pi^4 \to 2^{\frac{1}{3}}3(\sigma+1)\,[\sigma n\mathscr{T}_1/(\sigma+1)]^{\frac{4}{3}}$ as $\mathscr{T}_1^2 \to \infty$. (The above results do not obtain for $\sigma = 0$, but this case is physically uninteresting and will not be considered.)

The remainder of the discussion will be confined to the lowest eigenvalue, i.e. to the case $n = 1$.

When p_0 is imaginary, the coefficient of p_0 in (2.16) is real and positive. From (2.4), we find that

$$p_i^2 = \pi^4(\alpha^2+1)^2\,(\sigma^2+2\sigma)+\frac{\sigma}{\alpha^2+1}(\mathscr{T}^2\sigma-\alpha^2\lambda_0) \geqslant 0,$$

or, using (2.17), that

$$p_i^2 = -\sigma^2\pi^4(\alpha^2+1)^2+\frac{\mathscr{T}^2\sigma^2(1-\sigma)}{(\alpha^2+1)\,(1+\sigma)} \geqslant 0. \tag{2.19}$$

Therefore, a necessary condition for overstability is

$$\mathscr{T}_1^2 \geqslant \frac{\sigma+1}{-\sigma+1}(\alpha^2+1)^3. \tag{2.20}$$

Eliminating $\mathscr{T}_1^2$ from (2.18) and the equality of (2.20), we can find the value of α^2 at which overstability can just occur, i.e. when $p_i = 0$. This value satisfies

$$(2-3\sigma^2)\,\alpha^2+3(1-2\sigma^2)\,\alpha^4-3\sigma^2\alpha^2-1 = 0. \tag{2.21}$$

When $\sigma = \sqrt{\frac{2}{3}}$, $\alpha^2 = \infty$. Therefore $\sigma = \sqrt{\frac{2}{3}}$ represents the (upper) limiting value of the Prandtl number for which overstability can occur.*

Equation (2.17) together with (2.18) determines the minimum value of λ_0 for each pair of values of $\mathscr{T}_1^2$ and σ. The curves in figure 5 show the dependence of λ_0/π^4 on $\mathscr{T}_1^2$ for a number of values of σ. The curve C corresponds to steady convective instability.

It is possible, of course, that the fluid may become unstable in a steady convective manner and that overstability may occur in finite amplitude or that overstability may occur first and convection be preferred in finite amplitude. Figure 6 shows three divided regions in the $(\sigma, \mathscr{T}_1^2)$-plane. In region A overstability cannot arise because (2.20) cannot be satisfied. In region B convection occurs first but overstability may be the preferred state in finite amplitude.

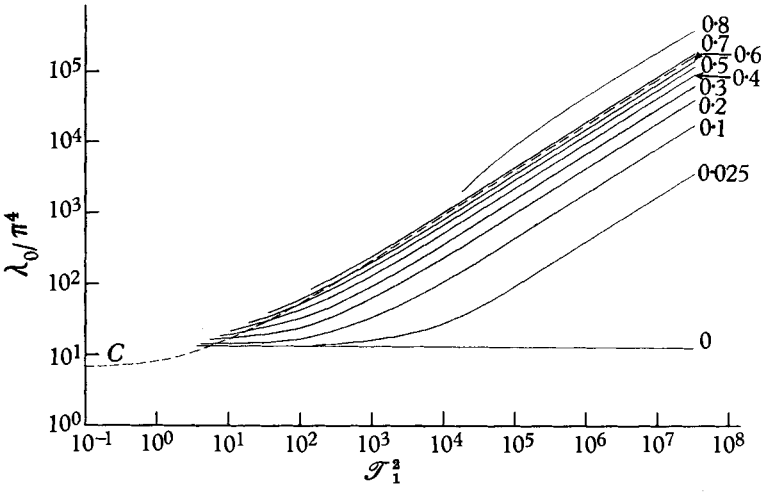

FIGURE 5. The λ_0/π^4 *vs* $\mathscr{T}_1^2$ relations for marginal stability. The dashed curve corresponds to steady convective instability. The solid curves correspond to instability in the form of time-periodic motions. The numbers on the curves are the values of the Prandtl numbers.

The curve between regions B and C marks the points at which overstability and convection occur simultaneously. The system will become overstable to infinitesimal disturbances when σ and $\mathscr{T}_1^2$ have values in the region C. Here, however, convection may come in at finite amplitude.

Why can overstability occur in the rotating systems and not when $\mathscr{T} = 0$? To answer this question we shall look into the energetics of the fluid.

For the two-dimensional case the solution to (2.1*c*) is

$$w_0 = 2\sqrt{2}\cos p_0 \tau \cos \pi\alpha x \sin \pi z, \tag{2.22}$$

where p_0^2 is equal to p_i^2 in (2.19). The remaining variables T_0, u_0, v_0 can be determined from equations (2.1) and are listed in § 4. If these expressions are substi-

* Nakagawa & Frenzen (III) show in figure 7 the value of λ_0 for overstability (R_c^* in their notation) in water ($\sigma \doteqdot 6$). That overstability cannot occur for $\sigma \geqslant \sqrt{\frac{2}{3}}$ is clear from the above argument. In addition, they derive the value $\lambda_0 = 2(\sigma+1)\,\alpha^{-2}\,(\alpha^2+1)^3$ when $\mathscr{T}_1^2 = 0$. However, condition (2.20) is violated so that this result is also incorrect.

tuted into the power integral expression (1.17) (with the right-hand side equal to zero), and if we use (2.19) for p_0^2, we have

$$\frac{\lambda_0/\pi^4}{(1+\sigma)\left[(\alpha^2+1)^2+\dfrac{\sigma^2}{(\sigma+1)^2}\dfrac{\mathscr{T}_1^2}{(\alpha^2+1)}\right]} = 2\frac{\alpha^2}{\alpha^2+1}, \tag{2.23}$$

where the left-hand side represents the rate of release of potential energy, $\{wT\}_m$, and the right-hand side the rate of dissipation of kinetic energy $\{\mathbf{v}.\nabla^2\mathbf{v}\}_m$. Equation (2.23) is equivalent to (2.17). Therefore the eigenvalue equation is a statement that a balance of the rate of viscous dissipation and the rate of release of potential energy is achieved by the fluid at the point of instability. The equivalent expression for the steady case is given by (2.5).

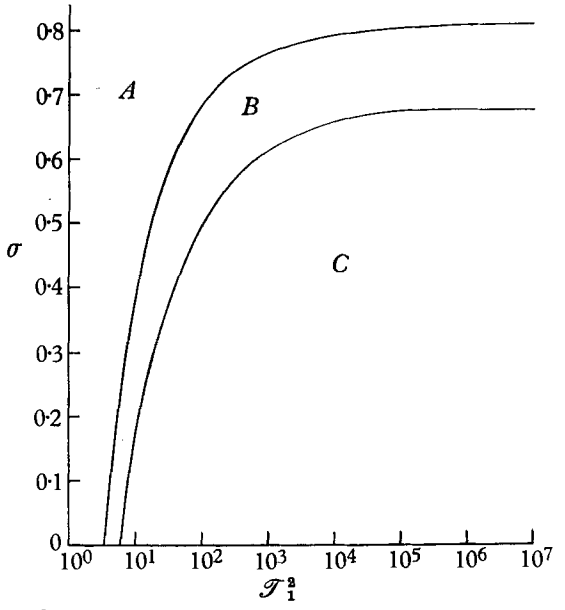

FIGURE 6. The $(\sigma, \mathscr{T}_1^2)$-plane is divided into three regions which are significant in the stability problem. In A instability occurs as steady convection. In B steady convective instability occurs first but overstability is possible for higher λ_0. In C overstability occurs before steady convection.

For fixed values of the convective heat transport, $\{wT\}_m$, and the rate of dissipation of kinetic energy, a decrease of σ in the overstable case reduces the effect of the external constraint $\mathscr{T}^2$. To compensate for the reduction of σ it is necessary that λ_0 be decreased. In the steady system the energy balance at the point of instability is unaltered by a change of σ. Therefore, in the overstable case, it is possible for the value of the Rayleigh number to be smaller than the value corresponding to the steady regime because the effect of the constraint is small when the Prandtl number is small.

From the stability problem, we have derived information concerning the onset of steady convective instability and of overstability. However, the amplitude of the motions for a given value of λ, the energetics of the fluid, the preferred

motions for a given set of external parameters, and still other features are unknowns which can be determined only in a finite-amplitude study. Therefore, we shall now go on to a study of finite-amplitude steady convection.

3. Finite-amplitude steady convection

The equations which govern steady convection are given by (1.3), (1.11), (1.13) and (1.14) with $\partial/\partial\tau \equiv 0$. Thus, the following equations are obtained by collecting terms in ϵ, ϵ^2 and ϵ^3 respectively: equations corresponding to ϵ^4, etc., can be found in the same way:

$$\left.\begin{aligned}
\mathscr{L}w_0 &\equiv \left[\nabla^6 + \mathscr{T}^2\frac{\partial^2}{\partial z^2} - \lambda_0\nabla_1^2\right]w_0 = 0.\\
\mathscr{L}w_1 &= \lambda_1\nabla_1^2 w_0 - \nabla^2 L_{00} + \mathscr{T}\frac{\partial Z_{00}}{\partial z} - \nabla_1^2 h_{00},\\
\mathscr{L}w_2 &= \lambda_2\nabla_1^2 w_0 + \lambda_1\nabla_1^2 w_1 - \nabla^2(L_{01}+L_{10}) + \mathscr{T}\frac{\partial}{\partial z}(Z_{01}+Z_{10})\\
&\quad - \nabla_1^2(h_{01}+h_{10}) + \sigma[\{w_0 T_0\}_m - \overline{w_0 T_0}]\nabla_1^2 w_0;
\end{aligned}\right\} \tag{3.1}$$

$$\left.\begin{aligned}
-\nabla^2 T_0 &= \sigma\lambda_0 w_0,\\
-\nabla^2 T_1 &= \sigma\lambda_0 w_1 + \sigma\lambda_1 w_0 - \sigma h_{00},\\
-\nabla^2 T_2 &= \sigma\lambda_0 w_2 + \sigma\lambda_1 w_1 + \sigma\lambda_2 w_0 + \sigma^2[\{w_0 T_0\}_m - \overline{w_0 T_0}]w_0 - \sigma(h_{01}+h_{10});
\end{aligned}\right\} \tag{3.2}$$

$$\left.\begin{aligned}
-\nabla^2\zeta_0 &= \mathscr{T}\frac{\partial w_0}{\partial z},\\
-\nabla^2\zeta_1 &= \mathscr{T}\frac{\partial w_1}{\partial z} - Z_{00},\\
-\nabla^2\zeta_2 &= \mathscr{T}\frac{\partial w_2}{\partial z} - (Z_{01}+Z_{10});
\end{aligned}\right\} \tag{3.3}$$

$$\frac{\partial u_i}{\partial x} + \frac{\partial v_i}{\partial y} + \frac{\partial w_i}{\partial z} = 0 \quad (i = 0, 1, 2, \ldots). \tag{3.4}$$

Here the subscripts i, j correspond to the order of the variables to be substituted into each expression: e.g. $h_{ij} = \mathbf{v}_i.\nabla T_j - \frac{\partial}{\partial z}(\overline{w_i T_j})$.

The method of solution is the same as the method used in the non-rotating problem (I). A brief outline of the method is given below.*

The form of w_0 can be determined by inspection from (3.1). Expressions for T_0, u_0 and v_0 are derived from the normalized expression for w_0 by means of equations (3.2), (3.3) and (3.4). The right-hand side of the second equation of (3.1) can then be computed directly since it is composed of zero-order functions only. However, two difficulties appear at this point. The inhomogeneous term in the w_1 equation will, in general, contain terms of the form of w_0 as well as the unknown parameter λ_1. In solving for the particular solution for w_1, one will obtain secular terms in addition to terms which are spatially periodic. In addition, the homogeneous solution of w_1 will contain the form of w_0 with an arbitrary amplitude.

* *Note added in proof.* A method for treating the finite-amplitude range has also been proposed by L. P. Gor'kov (1957). His method and that of Malkus & Veronis yield the same finite-amplitude results for λ_2.

Since λ_1 multiplies a term of the form of w_0 in the inhomogeneous term, we can evaluate λ_1 to cancel the remaining amplitudes of w_0. Secular terms are thereby eliminated and the assumed periodicity of the solution is maintained. Furthermore, by specifying that ϵ be the total amplitude of that part of w which contains w_0, we can write $\{ww_0\}_m = \epsilon$ or $\{w_i w_0\}_m = 0$ for $i > 0$, i.e. the homogeneous part of $w_i\,(i > 0)$ which has the form of w_0 has zero amplitude. The system of equations can now be solved for the w_i, T_i, u_i, v_i and λ_i. We shall apply the method first to determine an approximate finite-amplitude solution for the two-dimensional rolls. Though this case is unrealistic, it is the only case which, with a reasonable amount of effort, can be carried beyond the second approximation. Because the roll is not truly descriptive of the actual physical system, we shall discuss certain qualitative features of this case only. Later, in the analysis for the square cell, additional observable features of the flow will be presented.

(*a*) *Rolls*

The solution to the stability problem is given by equations (2.7) and (2.8). This is

$$\left.\begin{aligned} w_0 &= 2\cos\pi\alpha x \sin\pi z, & T_0 &= \frac{2\sigma\lambda_0}{\pi^2(\alpha^2+1)}\cos\pi\alpha x\sin\pi z,\\ u_0 &= -\frac{2}{\alpha}\sin\pi\alpha x\cos\pi z, & v_0 &= \frac{2\mathscr{T}_1}{\alpha(\alpha^2+1)}\sin\pi\alpha x\cos\pi z, \end{aligned}\right\} \tag{3.5}$$

where the value of α corresponding to a given value of $\mathscr{T}_1$ is given by (2.6), and λ_0 is given by (2.5)

The inhomogeneous term for w_1 can be evaluated directly; thus

$$Z_{00} = \frac{\partial}{\partial x}(\mathbf{v}_0.\nabla v_0) - \frac{\partial}{\partial y}(\mathbf{v}_0.\nabla u_0) = -\frac{4\mathscr{T}}{\alpha^2+1}\cos 2\pi\alpha x,$$

$$L_{00} = \frac{\partial}{\partial z}\left[\frac{\partial}{\partial x}(\mathbf{v}_0.\nabla u_0) + \frac{\partial}{\partial y}(\mathbf{v}_0.\nabla v_0)\right] - \nabla_1^2(\mathbf{v}_0.\nabla w_0) = 0,$$

$$h_{00} = \mathbf{v}_0.\nabla T_0 - \frac{\partial}{\partial z}(\overline{w_0 T_0}) = 0.$$

Therefore, $\mathscr{L}w_1 = -\pi^2\alpha^2\lambda_1 w_0$.

Now λ_1 is evaluated so as to cancel the form of w_0 from the right-hand side. Since the only term containing the form of w_0 is $\lambda_1\nabla_1^2 w_0$, it is necessary that $\lambda_1 = 0$. Thus,

$$\lambda_1 = 0, \quad w_1 = 0, \quad T_1 = 0, \quad u_1 = 0. \tag{3.6}$$

The second equation of (3.3) gives

$$v_1 = \frac{\mathscr{T}_1}{2\pi\alpha^3(\alpha^2+1)}\sin 2\pi\alpha x. \tag{3.7}$$

To solve for w_2, we note that $L_{01} = L_{10} = h_{01} = h_{10} = Z_{10} = 0$, and

$$\mathscr{T}\frac{\partial Z_{01}}{\partial z} = \frac{\mathscr{T}^2}{\alpha^2(\alpha^2+1)}[3\cos 3\pi\alpha x - \cos\pi\alpha x]\sin\pi z,$$

$$\sigma[\{w_0 T_0\}_m - \overline{w_0 T_0}]\nabla_1^2 w_0 = -\frac{\alpha^2\sigma^2\lambda_0}{\alpha^2+1}\cos\pi\alpha x(\sin 3\pi z - \sin\pi z),$$

$$\lambda_2\nabla_1^2 w_0 = -2\pi^2\alpha^2\lambda_2\cos\pi\alpha x\sin\pi z.$$

Thus, $$\mathscr{L}w_2 = \left[-2\pi^2\alpha^2\lambda_2 + \frac{\alpha^2\sigma^2\lambda_0}{\alpha^2+1} - \frac{\mathscr{T}^2}{\alpha^2(\alpha^2+1)}\right]\cos\pi\alpha x \sin\pi z + \frac{3\mathscr{T}^2}{\alpha^2(\alpha^2+1)}\cos 3\pi\alpha x \sin\pi z - \frac{\alpha^2\sigma^2\lambda_0}{\alpha^2+1}\cos\pi\alpha x \sin 3\pi z. \quad (3.8)$$

The first term on the right-hand side has the form of w_0 and must vanish. Hence,

$$\lambda_2 = \frac{\sigma^2\lambda_0}{2\pi^2(\alpha^2+1)} - \frac{\mathscr{T}^2}{2\pi^2\alpha^4(\alpha^2+1)}. \quad (3.9)$$

The evaluation of λ_2 provides the first finite-amplitude result. From the expression (1.9) for the heat transport, we can write

$$\frac{H}{\kappa\beta_m} = 1 + \frac{\sigma}{\lambda}\{wT\}_m, \quad (3.10)$$

where w and T are non-dimensional. Expanding w and T as in (1.15), we have

$$\{wT\}_m = \epsilon^2[\{w_0T_0\}_m + \epsilon\{w_0T_1 + w_1T_0\}_m + \epsilon^2\{w_0T_2 + w_1T_1 + w_2T_0\}_m + \epsilon^3\{w_0T_3 + w_1T_2 + w_2T_1 + w_3T_0\}_m + \epsilon^4\{w_0T_4 + w_1T_3 + w_2T_2 + w_3T_1 + w_4T_0\}_m + \ldots]. \quad (3.11)$$

Therefore, to the ϵ^2 approximation for the convective heat transport, we get

$$\frac{\sigma}{\lambda}\{wT\}_m = \frac{\sigma}{\lambda}\epsilon^2\{w_0T_0\}_m. \quad (3.12)$$

To the same approximation (1.16) becomes

$$\epsilon^2 = \frac{\lambda - \lambda_0}{\lambda_2}. \quad (3.13)$$

Hence,

$$\frac{\sigma}{\lambda}\{wT\}_m = \frac{\sigma}{\lambda_2}\left(1 - \frac{\lambda_0}{\lambda}\right)\{w_0T_0\}_m = \frac{\sigma^2\lambda_0}{\pi^2(\alpha^2+1)\lambda_2}\left(1 - \frac{\lambda_0}{\lambda}\right). \quad (3.14)$$

We can see from (3.14) that to the ϵ^2 approximation the convective heat transport varies inversely as λ_2. Table 1 contains values of the convective heat transport $\sigma\{wT\}_m/(\lambda - \lambda_0)$ of rolls for various values of σ and $\mathscr{T}_1^2$. The range of σ is restricted to the values for which overstability can also occur. Not that λ_2 and therefore $\sigma\{wT\}_m/(\lambda - \lambda_0)$ are negative for small Prandtl numbers and positive for larger values. In most of the range where λ_2 is negative overstability will occur before steady convection. However, for sufficiently low rotation rates, overstability cannot arise and the flow will be steady.

Since $\epsilon^2 > 0$, it is clear from (3.13) that negative λ_2 implies that $\lambda < \lambda_0$. According to this analysis, which is pivoted about the linear stability problem,

the system will behave as follows. As λ increases toward λ_0, heat is transported by pure conduction (figure 7). When $\lambda = \lambda_0$ convection will occur but now λ can be decreased below λ_0 and convection will be maintained. According to the ϵ^2 approximation, one could decrease λ indefinitely and convection would continue; therefore, one must go to a higher approximation to determine when the curve begins to turn up again.

	$\mathscr{T}_1^2$					
σ	0·1	0·5	1	5	10	10^2
0·025	−0·0239	−0·00702	−0·00487	−0·00377	−0·00406	−0·00724
0·1	−0·569	−0·117	−0·0808	−0·0619	−0·0671	−0·122
0·2	−6·01	−0·562	−0·365	−0·274	−0·0299	−0·600
0·3	4·87	−1·94	−1·07	−0·735	−0·827	−2·16
0·4	2·99	−14·36	−3·24	−1·81	−2·17	−24·2
0·5	2·54	7·39	−63·0	−5·60	−8·68	6·51
0·6	2·34	4·06	7·10	40·1	13·7	3·85
0·687	2·25	3·26	4·41	6·77	5·75	3·16
0·7	2·23	3·19	4·23	6·56	5·37	3·09
0·8	2·18	2·80	3·37	4·40	3·86	2·74

	$\mathscr{T}_1^2$					
σ	10^3	10^4	10^5	10^6	10^7	10^8
0·025	−0·0150	−0·0326	−0·0715	−0·168	−0·382	−1·06
0·1	−0·270	−0·690	−2·47	11·2	3·28	2·44
0·2	−1·82	77·6	3·66	2·55	2·21	2·09
0·3	29·6	3·53	2·50	2·23	2·09	2·04
0·4	4·20	2·64	2·25	2·14	2·05	2·02
0·5	3·01	2·37	2·16	2·10	2·03	2·01+
0·6	2·60	2·25	2·11	2·07	2·02	2·01−
0·687	2·43	2·18	2·09	2·04	2·01+	2·01−
0·7	2·41	2·16	2·08	2·03	2·01	2·01−
0·8	2·29	2·14	2·06	2·02	2·01−	2·00+

TABLE 1. Values of $\dfrac{\sigma\{wT\}_m}{\lambda-\lambda_0} = \dfrac{\sigma^2\lambda_0}{\pi^2(\alpha^2+1)\lambda_2}$ for rolls.

Experimentally, one would not observe the sequence of events described above. If a finite-amplitude perturbation were present, the system would become unstable at λ_U (figure 7), and the motions would grow very quickly from C to A, i.e. until the fluid transported the amount of heat corresponding to point A. A further increase in λ would be needed to increase H. On the other hand, if no finite-amplitude disturbance were present, instability would occur at λ_0, but the motions would grow very rapidly with $\lambda = \lambda_0$ until the heat transport corresponded to point B. If the system were allowed to 'run down', i.e. if λ were decreased from a value above λ_0, then the system would always follow the path *BACO*.

The onset of instability as a finite-amplitude disturbance in the rotating system marks a definite point of departure from the results of the non-rotating

system. In the latter case, convective heat transport is possible only for values of $\lambda > \lambda_0$. Why does the rotating system respond so differently in finite amplitude? What is the mechanism for the occurrence of finite amplitude instability?

The answers to these questions can be found in equation (1.14). For the steady convective case, we have

$$\nabla^6 w + \mathscr{T}^2 \frac{\partial^2 w}{\partial z^2} - \lambda \nabla_1^2 w = \sigma[\{wT\}_m - \overline{wT}]\nabla_1^2 w + \mathscr{T}\frac{\partial Z}{\partial z} - \nabla_1^2 h - \nabla^2 L. \quad (3.15)$$

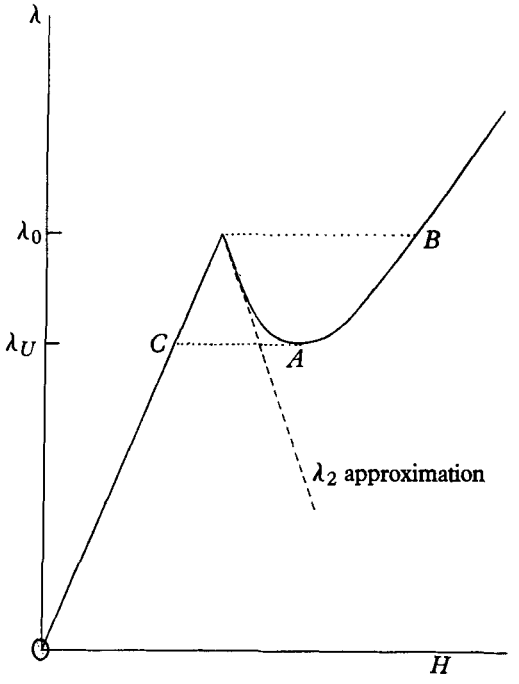

FIGURE 7. The λ *vs* H curve when λ_2 is negative.

The term $$Z = \frac{\partial}{\partial x}(\mathbf{v}.\nabla v) - \frac{\partial}{\partial y}(\mathbf{v}.\nabla u)$$

can be written in the form

$$Z = \mathbf{v}_1.\nabla_1\zeta - \boldsymbol{\omega}_1.\nabla_1 w = \nabla_1.[\mathbf{v}_1\zeta - \boldsymbol{\omega}_1 w], \quad (3.16)$$

where the subscript 1 corresponds to the horizontal vectors and $\boldsymbol{\omega}_1$ is the horizontal vorticity vector. If the term $\mathscr{T}(\partial Z/\partial z)$ is taken to the left-hand side of the equation (3.15), the second term can be written (with the aid of (1.3))

$$\mathscr{T}\frac{\partial}{\partial z}\nabla_1.\{\mathbf{v}_1\mathscr{T} - \mathbf{v}_1\zeta + \boldsymbol{\omega}_1 w\}. \quad (3.17)$$

The individual terms within the brackets correspond respectively to the horizontal transport of imposed vertical vorticity, the horizontal transport of local

vertical vorticity, and the vertical transport of horizontal vorticity. In finite amplitude, therefore, the fluid can generate a local vorticity whose net effect is to decrease the role of the constraining first term in (3.17). When the viscosity is large, the generation of local vorticity is accompanied by strong viscous dissipation so that the non-linear terms will stabilize the system.

It is important to note that the possibility of a finite-amplitude instability is brought about by interactions of the zero-average non-linear terms which do not contribute *per se* to the distortion of the mean temperature profile. These terms play an increasingly important role as the Prandtl number diminishes. In the non-rotating system, the heat transport curve of a fluid with small Prandtl number breaks away from the conduction line with a slope one-third greater than that of pure conduction, whereas when the Prandtl number is large the slope of the heat transport curve is twice the conduction slope. When an external constraint is present, the heat convected by the fluid varies as a function of the constraint.

When λ_2 is positive, heat is transported by convection only when λ is increased beyond λ_0. We shall discuss this case in some detail in a subsection on square cells.

When $\lambda_2 < 0$, it is necessary to consider the next approximation in order to find the point at which the λ *vs* H curve turns upward. We can feel fairly confident that the ϵ^2 approximation is valid only in a very limited range, otherwise the λ, H curve would cross the H axis, i.e. the fluid would transport a finite amount of heat in the absence of a temperature gradient.

λ_4 *for rolls.* Because of the vertical symmetry, $\lambda_i = 0$ for odd i. Hence, it is necessary to go to the ϵ^4 approximation to determine the higher-order effect on the heat transport.

The equations governing the ϵ^4 approximation can be determined from equation (3.15) and from the expansions (1.15) and (1.16). The results only will be listed here:

$$\left.\begin{aligned} w_2 &= w_{20}\cos\pi\alpha x\sin 3\pi z + w_{21}\cos 3\pi\alpha x\sin\pi z,\\ T_2 &= \frac{\sigma\lambda_0 w_{20}+\sigma^2 N_0}{\pi^2(\alpha^2+9)}\cos\pi\alpha x\sin 3\pi z + \frac{\sigma\lambda_0 w_{21}}{\pi^2(9\alpha^2+1)}\cos 3\pi\alpha x\sin\pi z\\ &\qquad - \frac{\sigma\mathscr{T}_1^2}{\alpha^4(\alpha^2+1)^2}\cos\pi\alpha x\sin\pi z; \end{aligned}\right\} \tag{3.18}$$

$$\left.\begin{aligned} \lambda_3 &= 0,\\ \lambda_4 &= -\frac{\sigma^2}{4}\left[\frac{\mathscr{T}_1^2}{\alpha^4(\alpha^2+1)^2}+\frac{\sigma^2 N_0}{\alpha^2+9}\left(\frac{\alpha^2\lambda_0/\pi^4}{A}+1\right)\right]\\ &\qquad -\frac{\sigma^4 N_0^2\alpha^2}{2A}+\frac{\mathscr{T}_1^2}{4\alpha^6(\alpha^2+1)}\left[\frac{1}{9\alpha^2+1}\left(1-\frac{\mathscr{T}_1^2}{B}\right)+\frac{1}{\alpha^2+1}\right], \end{aligned}\right\} \tag{3.19}$$

where $$w_{20} = \frac{\sigma\alpha^2 N_0}{\pi^4 A},\quad w_{21} = -\frac{3\mathscr{T}_1^2}{\pi^2\alpha^2(\alpha^2+1)B},\quad N_0 = \frac{\lambda_0}{\pi^2(\alpha^2+1)},$$

$$A = (\alpha^2+9)^3+9\mathscr{T}_1^2-\alpha^2\frac{\lambda_0}{\pi^4},\quad B = (9\alpha^2+1)^3+\mathscr{T}_1^2-9\alpha^2\frac{\lambda_0}{\pi^4}$$

Values of λ_4 for mercury ($\sigma = 0{\cdot}025$) and air ($\sigma = 0{\cdot}687$) are given in table 2.

We can now determine the range of validity of the ϵ^2 approximation. To the ϵ^4 approximation, (1.16) becomes

$$\epsilon^2 = -\frac{\lambda_2 + \sqrt{[\lambda_2^2 + 4\lambda_4(\lambda - \lambda_0)]}}{2\lambda_4}, \tag{3.20}$$

where the positive sign in front of the radical has been chosen so that $\epsilon^2 \to 0$ as $\lambda \to \lambda_0$. Only when $\lambda_2^2 > |4\lambda_4(\lambda - \lambda_0)|$ is the ϵ^2 approximation valid. From the values of λ_2 and λ_4 for air, $\lambda - \lambda_0 = -\frac{1}{4}\lambda_2^2/\lambda_4$ when $\lambda - \lambda_0 \doteqdot \lambda_0$ in the range $0 \leqslant \mathscr{T}_1^2 \leqslant 0{\cdot}1$. As $\mathscr{T}_1^2$ increases, the limiting value of $\lambda - \lambda_0$ decreases to $0{\cdot}03\lambda_0$ at $\mathscr{T}_1^2 \doteqdot 10$ and then asymptotically approaches $0{\cdot}16\lambda_0$. For mercury the value of $\lambda - \lambda_0$ beyond which the λ_4 approximation is no longer valid is λ_0 when $\mathscr{T}_1^2 = 0$, decreases to $0{\cdot}005\lambda_0$ when $\mathscr{T}_1^2 = 0{\cdot}5$, rises to $0{\cdot}14\lambda_0$ when $\mathscr{T}_1^2 = 10^4$ and then steadily decreases to $0{\cdot}09\lambda_0$ at $\mathscr{T}_1^2 = 10^8$. Therefore, the ϵ^4 approximation is valid for a rather limited range of λ. The λ_2 curve describes the system accurately in a slightly smaller range of λ.

$\mathscr{T}_1^2$	λ_4 (air)	λ_4 (mercury)	$\mathscr{T}_1^2$	λ_4 (air)	λ_4 (mercury)
0·1	0·0495	0·0971	10^3	−0·164	$0{\cdot}956 \times 10^{-2}$
0·5	0·168	0·286	10^4	−0·203	$0{\cdot}195 \times 10^{-2}$
1	0·230	0·354	10^5	−0·229	$0{\cdot}410 \times 10^{-3}$
5	0·122	0·277	10^6	−0·245	$0{\cdot}797 \times 10^{-4}$
10	0·042	0·196	10^7	−0·253	$0{\cdot}168 \times 10^{-5}$
10^2	−0·101	0·0499	10^8	−0·257	$0{\cdot}280 \times 10^{-5}$

TABLE 2. λ_4 for rolls.

In the non-rotating system (I), the ϵ^2 approximation for rolls is accurate for $\lambda - \lambda_0 \leqslant \lambda_0$. The more limited range of validity of λ_2 for air in the rotating problem can be traced to the stability problem itself. The system becomes unstable to a disturbance with the form of the second mode, i.e. $\sin 2\pi z$, at a relatively smaller value of λ. It was shown in § 2 that $(\lambda_0)_{n=2}/(\lambda_0)_{n=1} \to (16)^{\frac{1}{3}} = 2{\cdot}52$ as $\mathscr{T}_1^2 \to \infty$, whereas in the non-rotating system the ratio equals 16. Since the finite-amplitude solution is based on the linear stability problem, it can describe the system only in the range in which the fluid is not unstable to other disturbances. This range is ten times smaller in the rotating case (for large $\mathscr{T}_1^2$); therefore the corresponding approximation is accurate in an equally limited range. This reasoning does not apply to mercury where λ_2 is negative. In this case, the range of validity of the second-order approximation must be limited for the reason mentioned earlier. Nor can we apply the above reasoning to account for the extremely small range of validity of the ϵ^2 approximation for air when $\mathscr{T}_1^2 \doteqdot 10$. As we shall see later, the fluid behaves quite differently for these smaller values of $\mathscr{T}_1^2$ than it does either for zero rotation or for higher rotation rates.

From the expressions for the heat transport (3.10) and (3.11), we have to fourth order

$$\frac{H}{\kappa\beta_m} = 1 + \frac{\sigma\epsilon^2}{\lambda}[\{w_0 T_0\}_m + \epsilon^2\{w_0 T_2\}_m], \tag{3.21}$$

where the remaining terms in (3.11) vanish. Therefore,

$$\frac{H}{\kappa\beta_m} = 1+\frac{\sigma\epsilon^2}{\lambda}\left[\frac{\sigma\lambda_0}{\pi^2(\alpha^2+1)}-\frac{\sigma\mathscr{T}_1^2}{2\alpha^4(\alpha^2+1)}\epsilon^2\right]. \tag{3.22}$$

For mercury, $\lambda_2 < 0$ and $\lambda_4 > 0$. Therefore, from (3.20), we note that the amplitude ϵ^2 increases as a result of the higher approximation. H increases with ϵ^2 so that the net effect of λ_4 is to turn the λ *vs* H curve (figure 7) toward the right, i.e. toward point A. In order to determine the actual behaviour of the system as the λ *vs* H curve is turned upward again, it would be necessary to consider the next approximation.

The most important result which we have obtained from this study of finite-amplitude convection for rolls is that fluids with a sufficiently small Prandtl number can become unstable to a finite-amplitude disturbance at a lower value of λ than λ_0. The non-linear vorticity generated by the finite-amplitude motions enables the fluid to reduce the effect of the external constraint and thereby become unstable at lower values of the external parameters.

(*b*) λ_2 *for rectangular cells*

Using the method outlined earlier, we can determine λ_2 for the rectangular cell. The detailed analysis is rather tedious and lengthy, so that only the results will be given.

The stability solution is

$$\left.\begin{aligned} w_0 &= 2\sqrt{2}\cos\pi lx\cos\pi my\sin\pi z, \quad T_0 = 2\sqrt{2}\,\sigma N_0\cos\pi lx\cos\pi my\sin\pi z,\\ u_0 &= -\left[\frac{2\sqrt{2}\,m\mathscr{T}_1}{\alpha^2(\alpha^2+1)}\cos\pi lx\sin\pi my+\frac{2\sqrt{2}\,l}{\alpha^2}\sin\pi lx\cos\pi my\right]\cos\pi z,\\ v_0 &= \left[\frac{2\sqrt{2}\,l\mathscr{T}_1}{\alpha^2(\alpha^2+1)}\sin\pi lx\cos\pi my-\frac{2\sqrt{2}\,m}{\alpha^2}\cos\pi lx\sin\pi my\right]\cos\pi z, \end{aligned}\right\} \tag{3.23}$$

where $2\sqrt{2}$ is the normalization constant for w_0, $N_0 = \dfrac{\lambda_0}{\pi^2(\alpha^2+1)}$ and $l^2+m^2 = \alpha^2$. Equations (2.5) and (2.6) again determine λ_0 and α^2 as functions of $\mathscr{T}_1$. The first-order functions are

$$\left.\begin{aligned} w_1 &= [a_1(l,m)\cos 2\pi lx + a_2(l,m)\cos 2\pi my]\sin 2\pi z,\\ T_1 &= [b_1(l,m)\cos 2\pi lx + b_2(l,m)\cos 2\pi my]\sin 2\pi z,\\ v_1 &= \left[\frac{a_1\mathscr{T}_1}{4l(l^2+1)}\sin 2\pi lx-\frac{a_2}{m}\sin 2\pi my\right]\cos 2\pi z+\frac{\mathscr{T}_1}{2\pi l\alpha^2(\alpha^2+1)}\sin 2\pi lx\\ &\qquad +\frac{l\mathscr{T}_1}{2\pi\alpha^4(\alpha^2+1)}\sin 2\pi lx\cos 2\pi my,\\ u_1 &= -\left[\frac{a_1}{l}\sin 2\pi lx+\frac{a_2\mathscr{T}_1}{4m(m^2+1)}\sin 2\pi my\right]\cos 2\pi z\\ &\qquad -\frac{\mathscr{T}_1}{2\pi m\alpha^2(\alpha^2+1)}\sin 2\pi my-\frac{m\mathscr{T}_1}{2\pi\alpha^4(\alpha^2+1)}\cos 2\pi lx\sin 2\pi my, \end{aligned}\right\} \tag{3.24}$$

where $\lambda_1 = 0,$

$$a_1(l,m) = \frac{\dfrac{8\pi^3 l^2 m^2 \sigma N_0}{\alpha^2} + \dfrac{32\pi^5 l^2 m^2 (l^2+1)}{\alpha^4}\left[\alpha^2 + 1 + \dfrac{\mathscr{T}_1^2}{(\alpha^2+1)^2}\right]}{-4\pi^6[16(l^2+1)^3 + \mathscr{T}_1^2 - l^2\lambda_0/\pi^4]},$$

$$b_1(l,m) = \sigma \frac{\lambda_0 a_1 - 2\pi\sigma N_0 m^2/\alpha^2}{4\pi^2(l^2+1)},$$

$$a_2(l,m) = \alpha_1(m,l), \quad b_2(l,m) = b_1(m,l).$$

From these zero- and first-order functions and from (3.1), an expression for λ_2 can be obtained:

$$\lambda_2 = \frac{\sigma^2 N_0}{2} - \frac{\pi}{2\alpha^2}(m^2 b_1 + l^2 b_2) + \frac{\pi^3}{2\alpha^4}(m^2 a_1 + l^2 a_2)\left[\frac{\mathscr{T}_1^2}{\alpha^2+1} - (\alpha^2+1)^2\right] + \frac{\mathscr{T}_1^2 \pi^3}{2\alpha^4}\left[\frac{l^2 a_2}{m^2+1} + \frac{m^2 a_1}{l^2+1} + \frac{3}{2\pi(\alpha^2+1)}\right]. \quad (3.25)$$

As a function of the parameters σ, $\mathscr{T}_1$ and the ratio l/m, expression (3.25) for λ_2 has a triply infinite set of values. We shall restrict our attention here to the values of $\mathscr{T}_1^2$ which were considered in the subsection on rolls. Furthermore, we shall consider only two values of σ, those corresponding to mercury ($\sigma = 0{\cdot}025$) and air ($\sigma = 0{\cdot}687$). The ratio l/m cannot be chosen arbitrarily, of course, for it is a parameter whose value is determined by the physics of the system. In order to decide which of the infinite number of values of l/m is chosen by the fluid we turn now to the relative stability criterion which was developed in I.

The relative stability criterion is the answer to the following question. If all of the mathematically possible solutions of a statistically steady physical system are known, which of the solutions is stable to disturbances which have the form of any of the other solutions? When all of the solutions are orthogonal to each other (as in the present case), the criterion takes a particularly simple form. The fluid chooses that solution which has the maximum value of $\{\beta^2\}_m$. From (1.10) in non-dimensional form, $\{\beta^2\}_m$ can be written

$$1 + \frac{\sigma^2}{\lambda^2}\{[\{wT\}_m - \overline{wT}]^2\}_m. \quad (3.26)$$

To the ϵ^2 approximation, (3.26) is equal to

$$1 + \frac{\sigma^2\epsilon^4}{\lambda^2}\{[\{w_0 T_0\}_m - \overline{w_0 T_0}]^2\}_m = 1 + \frac{\sigma^4 N_0^2 \epsilon^4}{2\lambda^2} = 1 + \frac{\sigma^4 N_0^2 (\lambda - \lambda_0)^2}{2\lambda^2 \lambda_2^2}, \quad (3.27)$$

where (3.13) was used to derive the last equality. Since N_0 is not a function of l/m, the solution with maximum $\{\beta^2\}_m$ at a given value of λ is the solution with minimum λ_2 or maximum heat transport.

For this problem λ_2 as given by (3.25) has a minimum at* $l/m = \infty$ for small $\mathscr{T}_1^2$ and at* $l/m = 1$ for large $\mathscr{T}_1^2$. The value of $\mathscr{T}_1^2$ at which the preferred shape crosses over from $l/m = \infty$ to $l/m = 1$ depends upon the Prandtl number. Values of the

* When $l/m = \infty$, the cellular geometry is that of limiting rectangles, i.e. the cells take the form of rolls in the limit. When $l/m = 1$, the cells are square.

convective heat transport for air and mercury are given in table 3 for square cells and for limiting rectangles.

A result which is immediately evident upon comparing tables 1 and 3 is that the value of the heat transport for limiting rectangles differs markedly from the value for rolls. This difference was found also in the non-rotating case. Again the only conclusion which we can draw from these results is that one must use the limiting rectangle in the description of the two-dimensional case. Though neither the roll nor the limiting rectangle can satisfy lateral experimental boundary conditions, nevertheless the limiting rectangle can approximate long thin rectangular cells.

	Air		Mercury			Air		Mercury	
$\mathscr{T}_1^2$	Square	LR	Square	LR	$\mathscr{T}_1^2$	Square	LR	Square	LR
0·1	1·15	1·20	0·00623	0·0155	10^3	1·95	1·11	−0·0448	0·00993
0·5	0·971	0·961	0·00340	0·00455	10^4	2·06	1·23	−0·0361	0·0209
1	0·900	0·862	0·00275	0·00322	10^5	2·05	1·29	−0·0587	0·0445
5	0·896	0·782	0·00262	0·00244	10^6	2·03	1·31	−0·118	0·0924
10	0·983	0·807	0·00329	0·00270	10^7	2·02	1·32	−0·249	0·184
10^2	1·49	1·02	0·0126	0·00481	10^8	2·01	1·33	−0·608	0·342

TABLE 3. Convective heat transport $(\sigma\{wT\}_m)/(\lambda-\lambda_0)$ for steady square cells and limiting rectangles.

An additional fact which emerges from a comparison of tables 1 and 3 is that for air the heat transport of squares exactly coincides with that of rolls when $\mathscr{T}_1^2$ is large. Whether this is a chance coincidence or has some deeper significance has not been determined. Clearly the physical factors which enter into the determination of λ_2 are quite different in the two cases.

A definite qualitative difference between the two-dimensional and three-dimensional cases is illustrated by the heat transport for mercury. For rolls a finite-amplitude instability can occur throughout the range of $\mathscr{T}_1^2$ considered, whereas limiting rectangles will not become unstable to finite-amplitude perturbations.

We may note from table 3 that steady convective instability in mercury will set in the form of limiting rectangles for the range $0 \leqslant \mathscr{T}_1^2 \leqslant 3$. For higher values of $\mathscr{T}_1^2$, convection occurs in the form of square cells. Since overstability can occur (though at a higher Rayleigh number) when $\mathscr{T}_1^2 \doteqdot 4$, further discussion about the expected nature of convection must be postponed until the finite-amplitude effects of overstability are presented.

One can predict the cellular structure of air over a much larger range of $\mathscr{T}_1^2$. It is evident from table 3 that limiting rectangles will be preferred only when $\mathscr{T}_1^2 < 0{\cdot}5$. Since overstability cannot set in until $\mathscr{T}_1^2 \doteqdot 108$, convection will take place in the form of steady square cells in the range $0{\cdot}5 \leqslant \mathscr{T}_1^2 \leqslant 108$.

It should be noted also that the very small amplitude of heat convection in mercury indicates that the heat transport curve in the H *vs* λ graph starts off practically tangent to the conduction line when instability occurs.

In air the convective heat transport is much larger than it is in mercury. An interesting property for air exhibited by table 3 is that the convective heat transport for both the limiting rectangle and the square approach asymptotic values for large $\mathscr{T}_1^2$. The asymptotic value for square cells is equal to the value for rolls. Furthermore, the non-rotating roll has precisely the same value $(\sigma\{wT\}_m/(\lambda-\lambda_0) = 2)$ for all fluids. The value of the heat transport for limiting rectangles at large $\mathscr{T}_1^2$, approaches the same value $\frac{4}{3}$ as it has in the non-rotating system.

The results for large $\mathscr{T}_1^2$ must be reconsidered in the light of finite-amplitude overstable motions. However, for small values of the Taylor number ($\leqslant 10^2$ for air, $\leqslant 10$ for mercury) it ought to be possible to check the above results experimentally. For instance, one ought to be able to see whether the limiting rectangle is actually the preferred cellular shape in air at very low rotation rates. The slope of the heat transport *vs* λ curve ought to be much steeper for low rotation rates than it is for zero rotation. Finally, the λ_4 values for rolls in air are positive when $\mathscr{T}_1^2$ is small. If this result bears even a qualitative significance to the realizable square or limiting rectangle, it would mean that for small $\mathscr{T}_1^2$ the heat transport is smaller than the value given by the λ_2 approximation.

To summarize the results of this section, we have found that in a fluid with a small Prandtl number it is possible that a finite-amplitude instability can occur before the fluid becomes unstable to infinitesimal perturbations. In this case, the finite-amplitude motions partially cancel the effect of the imposed constraint. For realizable cellular patterns in mercury this finite-amplitude instability will occur only in the range where overstability occurs first. It is, therefore, necessary to look into finite-amplitude overstable motions to determine whether the fluid can indeed be unstable to finite-amplitude disturbances.

4. Finite-amplitude overstable motions

In the analysis of these motions, the method of solution outlined in the previous section is inadequate. The difficulty which arises in the present case can be demonstrated by the following argument.

Let $w_0 = \cos p_0 \tau f(x,y)\, g(z)$ be the solution to (2.1 *c*). Then u_0, v_0 and T_0 can be determined from the remaining equations of (2.1). The inhomogeneous terms of the equations for w_1, w_2, etc., contain products of the lower-order functions, and the individual inhomogeneous terms are operated on by operators such as $(\partial/\partial\tau) - \nabla^2$. As a result, terms of the type $\sin p_0 \tau f(x,y)\, g(z)$ may appear as forcing terms but they do not contribute to the evaluation of the λ_i since they are orthogonal to the basic solution. Therefore, they remain as inhomogeneous terms and will give rise to secular terms in w_1, w_2, etc., because they satisfy the basic homogeneous equation. One cannot avoid the difficulty by introducing an arbitrary phase since the same difficulty arises regardless of the phase of the basic solution, i.e. out of phase components are always generated.

The present difficulty is not unique to the overstable problem. Indeed, one can conceive of examples in the steady problem in which the same problem arises. For example, in the basic roll solution, $w_0 = \cos \pi a x g(z)$, there are instances when a generated inhomogeneous term has the form $\sin \pi a x g(z)$. In the examples of the

previous section these 'resonant' terms always cancelled identically. However, it is possible that in some problems this fortuitous cancellation will not occur.

To reduce the equations to a soluble sequence once again we add an additional expansion. Specifically, let

$$\tau = t/p, \tag{4.1}$$

so that $\frac{\partial}{\partial \tau} = \frac{\partial}{\partial t}\frac{\partial t}{\partial \tau} = p\frac{\partial}{\partial t}$. We now expand p in powers of ϵ as

$$p = p_0 + \epsilon p_1 + \epsilon^2 p_2 + \ldots, \tag{4.2}$$

where the p_i are to be determined.

If we add (4.1) and (4.2) to the expansions (1.15) and (1.16), the equations (1.11), (1.13) and (1.14) take the form (where we give only the ϵ^1 terms (a) and ϵ^2 terms (b))

$$\mathscr{L}w_0 \equiv \left[\left(\frac{p_0}{\sigma}\frac{\partial}{\partial t} - \nabla^2\right)^2 \left(p_0\frac{\partial}{\partial t} - \nabla^2\right)\nabla^2 + \mathscr{T}^2\left(p_0\frac{\partial}{\partial t} - \nabla^2\right)\frac{\partial^2}{\partial z^2} - \lambda_0\left(\frac{p_0}{\sigma}\frac{\partial}{\partial t} - \nabla^2\right)\nabla_1^2\right] w_0 = 0, \tag{4.3a}$$

$$\begin{aligned}\mathscr{L}w_1 = -\Bigg\{p_1\left[\frac{3p_0^2}{\sigma^2}\frac{\partial^3}{\partial t^3} - 2p_0\left(\frac{1}{\sigma^2} + \frac{2}{\sigma}\right)\frac{\partial^2}{\partial t^2}\nabla^2 + \left(1 + \frac{2}{\sigma}\right)\frac{\partial}{\partial t}\nabla^4\right]\nabla^2 + p_1\frac{\partial}{\partial t}\left(\mathscr{T}^2\frac{\partial^2}{\partial z^2} - \frac{\lambda_0}{\sigma}\nabla_1^2\right)\\ - \lambda_1\left(\frac{p_0}{\sigma}\frac{\partial}{\partial t} - \nabla^2\right)\nabla_1^2\Bigg\} w_0 + \mathscr{T}\left(p_0\frac{\partial}{\partial t} - \nabla^2\right)\frac{\partial Z_{00}}{\partial z} - \left(\frac{p_0}{\sigma}\frac{\partial}{\partial t} - \nabla^2\right)\nabla_1^2 h_{00}\\ + \left(p_0\frac{\partial}{\partial t} - \nabla^2\right)\left(\frac{p_0}{\sigma}\frac{\partial}{\partial t} - \nabla^2\right)L_{00};\end{aligned} \tag{4.3b}$$

$$\left(\frac{p_0}{\sigma}\frac{\partial}{\partial t} - \nabla^2\right)\zeta_0 = \mathscr{T}\frac{\partial w_0}{\partial z}, \tag{4.4a}$$

$$\left(\frac{p_0}{\sigma}\frac{\partial}{\partial t} - \nabla^2\right)\zeta_1 = \mathscr{T}\frac{\partial w_1}{\partial z} - \frac{p_1}{\sigma}\frac{\partial \zeta_0}{\partial t} - Z_{00}; \tag{4.4b}$$

etc.

$$\left(p_0\frac{\partial}{\partial t} - \nabla^2\right)T_0 = \sigma\lambda_0 w_0, \tag{4.5a}$$

$$\left(p_0\frac{\partial}{\partial t} - \nabla^2\right)T_1 = \sigma\lambda_0 w_1 - p_1\frac{\partial T_0}{\partial t} + \sigma\lambda_1 w_0 - \sigma h_{00}; \tag{4.5b}$$

etc.

The continuity equation has the form (3.4).

One can now proceed in the same manner as in the steady case. However, both sets of undetermined coefficients p_i and λ_i are used to eliminate the resonant terms whose forms are $\cos tf(x,y)\,g(z)$ and $\sin tf(x,y)\,g(z)$. Using this method we find that the frequency p of the overstable oscillation changes with amplitude. It is clear that if out-of-phase resonant terms had been generated in the steady case, one would have had to expand α in powers of ϵ, i.e. the basic spatial wave number would have been a direct function of amplitude also.

The algebra involved in the solution of the overstable case is so extremely tedious and lengthy that only the solution to the stability problem and the method of procedure will be outlined here. The expressions for w_1, T_1, etc., and for λ_2, p_2 will not be written explicitly.

For the general rectangle, the solution of the stability problem is*

$$\left.\begin{aligned}
w_0 &= 4\cos t\cos\pi lx\cos\pi my\sin\pi z,\\
T_0 &= \frac{4\pi^2\sigma\lambda_0/\pi^4}{p_0^2/\pi^4+(\alpha^2+1)^2}[(\alpha^2+1)\cos t+p_0/\pi^2\sin t]\cos\pi lx\cos\pi my\sin\pi z,\\
u_0 &= -4\Big\{\frac{l}{\alpha^2}\cos t\sin\pi lx\cos\pi my\\
&\qquad +\frac{m}{\alpha^2}\mathscr{T}_1\frac{[\sigma^2(\alpha^2+1)\cos t+\sigma(p_0/\pi^2)\sin t]}{p_0^2/\pi^4+\sigma^2(\alpha^2+1)^2}\cos\pi lx\sin\pi my\Big\}\cos\pi z,\\
v_0 &= 4\Big\{\frac{l}{\alpha^2}\mathscr{T}_1\frac{\sigma^2(\alpha^2+1)\cos t+\sigma(p_0/\pi^2)\sin t}{p_0^2/\pi^4+\sigma^2(\alpha^2+1)^2}\sin\pi lx\cos\pi my\\
&\qquad -\frac{m}{\alpha^2}\cos t\cos\pi lx\sin\pi my\Big\}\cos\pi z.
\end{aligned}\right\}\tag{4.6}$$

The inhomogeneous term in (4.3b) can be determined as a function of p_1, λ_1 and the remaining (known) parameters of the problem. We now have an expression with non-resonant forcing terms plus terms of the type

$$[(ap_1+b\lambda_1+c)\cos t+(dp_1+e\lambda_1+f)\sin t]\cos\pi lx\cos\pi my\sin\pi z.$$

The coefficients a, b, c, d, e and f are functions of previously determined parameters. One evaluates p_1 and λ_1 so that the coefficients of the resonant term vanish. It is then possible to go on and determine the higher order λ_i and p_i in the same manner.

As in the steady case, λ_1 vanishes and $p_1\equiv 0$ here. Therefore, we must consider ϵ^2 terms to determine the first finite-amplitude effects. This evaluation was carried out for the case of the general rectangle and numerical results were computed for square cells and limiting rectangles in air and mercury. The results for the convection heat transport (as given by the ϵ^2 approximation (3.14)) for overstability are shown in table 4.

A comparison of the values of the convective heat transport for air in tables 3 and 4 indicates that heat is convected in air by steady cellular motions for $\mathscr{T}_1^2<10^6$. However, for $\mathscr{T}_1^2\geqslant 10^6$, overstable oscillations with a cellular pattern of squares will become the preferred motion *in finite amplitude* even though instability occurs as steady convection. The preference for overstability is very slight, and experimentally one may expect either type of motion to occur. The sequence of preferred finite-amplitude motions in air is: steady convective

* We can, of course, include arbitrary phases in the horizontal co-ordinate dependence and in the time dependence. However, no loss of generality is involved in writing the solution as given by (4.6). The ensemble average is now an average over the horizontal space and time periods, i.e. $\dfrac{1}{8\pi lm}\displaystyle\int_{-l}^{l}\int_{-m}^{m}\int_{0}^{2\pi}\{\ \}\,dx\,dy\,dt.$

limiting rectangles for $\mathscr{T}_1^2 < 0{\cdot}5$, steady convective squares for $0{\cdot}5 \leqslant \mathscr{T}_1^2 < 10^6$, and overstable square cells for $\mathscr{T}_1^2 \geqslant 10^6$.

The cross-over from steady convection to overstability in mercury takes place at lower values of $\mathscr{T}_1^2$ and is indeed much more definite. As we noted earlier, steady limiting rectangles occur for $\mathscr{T}_1^2 < 3$ and the system changes over to

	Mercury		Air	
$\mathscr{T}_1^2$	Square	LR	Square	LR
5	0·00416	0·0016	—	—
10	0·00431	0·00303	—	—
10^2	0·0136	0·0207	—	—
10^3	0·0394	0·0444	1·14	1·31
10^4	0·0733	0·0728	1·66	1·55
10^5	0·107	0·105	1·95	1·59
10^6	0·128	0·126	2·07	1·60
10^7	0·138	0·136	2·13	1·61
10^8	0·146	0·144	2·16	1·62

TABLE 4. Convective heat transport for overstable square cells and limiting rectangles.

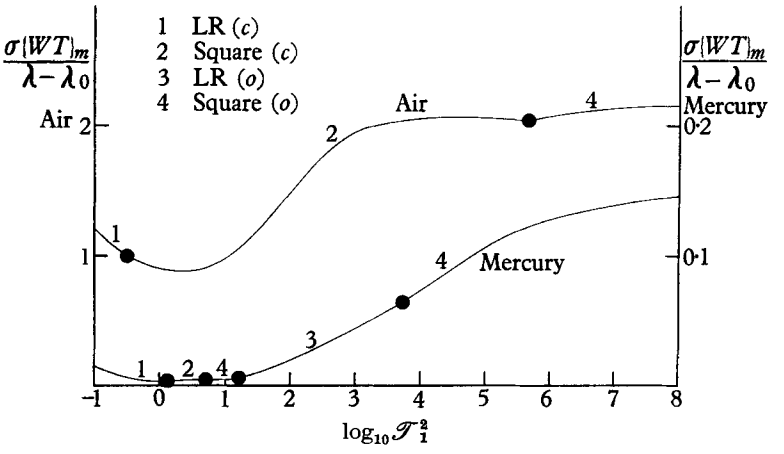

FIGURE 8. The convective heat transport values for air and mercury as functions of $\mathscr{T}_1^2$. The numbers on the portions of the curves lying between the dots mark the type of convective motions which occur in the specified ranges of $\mathscr{T}_1^2$. (*c*) corresponds to steady convective motions, (*o*) to overstable motions.

steady square cells when $\mathscr{T}_1^2 \geqslant 3$. Overstable square cells are preferred when $\mathscr{T}_1^2 \doteqdot 4{\cdot}5$ and remain as the preferred motion until $\mathscr{T}_1^2 \doteqdot 20$. However, at this point overstable limiting rectangles come in and are preferred to squares until $\mathscr{T}_1^2 \doteqdot 7 \times 10^3$, when overstable square cells become preferred again. These results are summarized in figure 8. It should be noted that the preference for square cells over limiting rectangles at large Taylor numbers is based on a very small

difference in heat transport (1 to 2 %). It may therefore be very difficult to obtain any recognizable stable pattern unless one were to make the determination at larger λ where higher order effects may conceivably solidify the preference.

The convective heat transport for mercury is a small fraction of the conductive heat transport throughout the range of $\mathscr{T}_1^2$ considered, and one may expect the H *vs* λ curve for $\lambda \geqslant \lambda_0$ to be practically tangent to the conduction line until higher order effects become important. In air the heat transport curve breaks away quite sharply after instability and has about twice the slope of the pure conduction line.

	Mercury		Air	
$\mathscr{T}_1^2$	Square	LR	Square	LR
5	11·3	0·735	—	—
10	2·30	1·80	—	—
10^2	0·332	1·18	—	—
10^3	$6{\cdot}28 \times 10^{-2}$	0·263	−2·14	1·33
10^4	$5{\cdot}46 \times 10^{-3}$	$6{\cdot}03 \times 10^{-2}$	−1·16	0·466
10^5	$-2{\cdot}48 \times 10^{-3}$	$2{\cdot}13 \times 10^{-2}$	−0·558	0·160
10^6	$-1{\cdot}93 \times 10^{-3}$	$8{\cdot}61 \times 10^{-3}$	−0·292	0·0616
10^7	$-9{\cdot}91 \times 10^{-4}$	$4{\cdot}20 \times 10^{-3}$	−0·138	0·0260
10^8	$-5{\cdot}80 \times 10^{-4}$	$1{\cdot}80 \times 10^{-3}$	−0·0645	0·0115

TABLE 5. The coefficient $p_2\lambda_0/p_0\lambda_2$ for mercury and air.

One of the most important results in the finite-amplitude study of overstable convection is that neither mercury nor air become unstable to finite-amplitude perturbations. Since the overstable oscillations in mercury take place at a much lower value of λ_0 than does steady convective instability, the fact that the latter can become unstable to finite-amplitude perturbations will not be observed experimentally.

The finite-amplitude effects on the frequency of the oscillation can be determined by (4.2) which, to the ϵ^2 approximation, has the form

$$\frac{p}{\pi^2} = \frac{p_0}{\pi^2} + \frac{\epsilon^2}{\pi^2} p_2. \tag{4.7}$$

Using (3.13), equation (4.7) can be written

$$\frac{p}{\pi^2} = \frac{p_0}{\pi^2}\left\{1 + \frac{p_2\lambda_0}{p_0\lambda_2}\left(\frac{\lambda}{\lambda_0} - 1\right)\right\}. \tag{4.8}$$

The coefficient $p_2\lambda_0/p_0\lambda_2$ is shown in table 5 for air and mercury. When the change in the frequency is negative, the correction decreases the convective heat transport (since λ_2 is a function of p_2). One of the most surprising features exhibited by the change in the frequency is the magnitude of effect on the heat transport even when the change in the frequency is extremely small, as it is for higher rotation rates in mercury. Indeed, the value of λ_2 in mercury without the

p_2 correction is negative for $10^4 \leqslant \mathscr{T}_1^2 \leqslant 10^7$. The change in frequency causes λ_2 to become positive, and the system is stable to finite-amplitude perturbations. Thus, the non-linear change in frequency effectively stabilizes the system in this part of the range. Where p_2 is positive, the non-linear change in frequency makes the system less stable.

5. Summary and conclusions

The most important conclusion in the stability investigation is that overstability occurs because the fluid is thereby able to reduce the constraint of the imposed rotation. A second conclusion of considerable interest is that in steady convective instability the wavelength of the cell measured along the boundary (as it is distorted by the rotation) is equal to the wavelength of the non-rotating cell. Other results (which are explicitly or implicitly contained in Chandrasekhar's original investigation (1953)) are that overstability cannot occur in a fluid with a Prandtl number greater than $\sqrt{\frac{2}{3}}$ because the rate of dissipation of kinetic energy always exceeds the rate of release of potential energy for larger σ, and that overstability cannot occur for sufficiently low rotation rates because the tendency of the fluid to undo the external constraint is more than offset by the increased dissipation due to the time-dependent motions.

For a range of the external parameters it is possible for the fluid, through finite-amplitude growth, to decrease the effect of the external constraint by generating a motion to counteract the effects of the imposed constraint. In cases where this happens, the fluid may become unstable to finite-amplitude disturbances before it becomes unstable to infinitesimal perturbations. Neither air nor mercury, the two fluids considered here, will exhibit this finite-amplitude behaviour under laboratory conditions.

More particular results in the finite-amplitude study are as follows. As the rotation rate is increased, the preferred cellular pattern for convection in air changes from steady limiting rectangles to steady squares to overstable squares (overstable square cells are preferred in finite amplitude even though the fluid first becomes unstable to steady convective motions). In mercury the sequence of preferred cellular shapes changes with increasing Taylor numbers from steady limiting rectangles, to steady squares, to overstable squares, to overstable limiting rectangles, and finally, when $\mathscr{T}_1^2 \doteq 10^6$, to overstable squares again. The heat convected by mercury after instability is only a small fraction of the conducted heat, and consequently the H *vs* λ curve will not show the very sharp breaks which are exhibited in the non-rotating system. In air the convective heat transport is at least as large as the conductive transport for all rotation rates, and the H *vs* λ curve will show a sharp break at the point of instability.

The frequency of the oscillations in overstable motions is a direct function of the amplitude. The change in frequency is too small to be noticeable in mercury when $\mathscr{T}_1^2 > 50$. However, even when small, the change in frequency has a marked effect on the heat transport.

According to the present investigation the fluid reacts to the imposed constraint by generating internal motions which counteract the external constraint. This result hints rather strongly that in general, when a fluid is subjected to

external constraints, it may generate motions which tend to offset the constraint.* In particular, in an electrically conducting fluid it is possible that a magnetic disturbance will grow so as to offset even further the constraint of the imposed rotation. In such a case the preferred convective state would be one with a self-generated magnetic field.

An additional suggested result with fairly broad application is the reason for the possible occurrence of a finite-amplitude instability. In other problems, such as shear flow in a channel, a finite amplitude instability can also occur (Meksyn & Stuart 1951). The one feature which these problems have in common is the dual role of viscosity mentioned in the introduction. Viscosity acts as an energy-releasing mechanism as well as a dissipative mechanism. Since finite-amplitude growth is invariably accompanied by increased viscous dissipation, one would not expect a finite-amplitude instability to occur unless the fluid were able to release even more potential energy. The fact that viscosity can fulfil the role as the energy-releasing mechanism suggests that this dual role of viscosity is essential to finite-amplitude instability.

It is interesting to note that the information concerning the appearance of a finite-amplitude instability is a consequence of an investigation which is pivoted about the linear stability problem. Application of the method described here to other problems, such as shear flow in a channel, may yield important results concerning the possible occurrence of finite-amplitude instability. One still feels, however, that the tools which we possess for treating finite-amplitude problems are woefully inadequate and that a more direct approach to non-linear stability problems should be sought.

A note should be added about an alternative, integral, technique for determining finite-amplitude effects. The method employed by Stuart (1958) and discussed in I is based on the power integral which can be derived by multiplying (1.11) by T and averaging. If quantities with the form of the stability solution are substituted into the power integral, one can then deduce the amplitude of w or T as a function of the external parameter λ. However, in the present problem this type of evaluation would yield results which are misleading because the principal effects in the determination of amplitude are those which result from the zero-average non-linear terms. These terms do not appear in the power integral.

Finally, what are the possible applications of these results to the fields of geophysics and astrophysics? (*a*) The formal technique described here together with the relative stability criterion provides a means for determining the

* The first finite-amplitude result (λ_2) for rolls was computed for an electrically conducting fluid subjected to heating from below and cooling from above and with an imposed magnetic field. As Chandrasekhar (1952) has shown, the imposed magnetic field acts as a constraint on the system in much the same manner as does the rotation. In the finite-amplitude computation, λ_2 is negative for a restricted range of the parameter η/κ, where η is the magnetic diffusivity. The range lies within the range of values of η/κ within which overstability can occur. Therefore, the possibility of finite amplitude instability exists also for this case, although it cannot occur in experiments realizable in the laboratory. The parametric values correspond to those which can exist in stellar atmospheres as Chandrasekhar has shown.

preferred finite-amplitude configuration of any statistically steady system with a solved stability problem. The principal limitation of the method lies in the formidable computations which may be required to carry out the analysis. (*b*) The very important role of viscosity as the energy releasing mechanism in a gyroscopically constrained system indicates that one ought to exercise some care in using such approximations as that of geostrophic flow in discussing the energetics of the fluid. (*c*) The ability of a fluid to react to externally imposed conditions may lead to a fuller understanding of the mechanistic behaviour of large-scale systems such as the atmosphere or the ocean.

A number of the ideas which are presented in this paper were a direct result of discussions with W. V. R. Malkus, and I wish to acknowledge his many valuable suggestions. The work was performed under the auspices of the Office of Naval Research and is Contribution no. 985 from the Woods Hole Oceanographic Institution.

REFERENCES

BOUSSINESQ, J. 1903 *Theorie Analytique de la Chaleur*, **2**, 172. Paris: Gauthier-Villars.

CHANDRASEKHAR, S. 1952 On the inhibition of convection by a magnetic field. *Phil. Mag.* (7), **43**, 501.

CHANDRASEKHAR, S. 1953 The instability of a layer of fluid heated below and subject to coriolis forces. *Proc. Roy. Soc.* A, **217**, 306.

CHRISTOPHERSON, D. G. 1940 *Quart. J. Math.* **11**, 63.

FULTZ, D. & NAKAGAWA, Y. 1955 *Proc. Roy. Soc.* A, **231**, 198.

GOR'KOV, L. P. 1957 *J. Exptl. Theor. Phys.* (*U.S.S.R.*), **33**, 402.

MALKUS, W. V. R. & VERONIS, G. 1958 Finite amplitude cellular convection. *J. Fluid Mech.* **4**, 225.

MEKSYN, D. & STUART, J. T. 1951 *Proc. Roy. Soc.* A, **208**, 517.

NAKAGAWA, Y. & FRENZEN, P. 1955 A theoretical and experimental study of cellular convection in rotating fluids. *Tellus*, **7**, 1.

STUART, J. T. 1958 On the non-linear mechanics of hydrodynamic stability. *J. Fluid Mech.* **4**, 1.